JOURNAL OF PETROLOGY | VOLUME 43 | NUMBER 11 | PAGES 2049–2074 | 2002

Partial Melting and Assimilation of Dolomitic Xenoliths by Mafic Magma: the Ioko-Dovyren Intrusion (North Baikal Region, Russia)

THOMAS WENZEL[1]*, LUKAS P. BAUMGARTNER[1], GERHARD E. BRÜGMANN[2], EDUARD G. KONNIKOV[3] AND EVGENIY V. KISLOV[4]

[1]INSTITUT FÜR GEOWISSENSCHAFTEN, JOHANNES GUTENBERG-UNIVERSITÄT, D-55099 MAINZ, GERMANY

[2]MAX PLANCK-INSTITUT FÜR CHEMIE, ABTEILUNG GEOCHEMIE, D-55020 MAINZ, GERMANY

[3]INSTITUTE OF EXPERIMENTAL MINERALOGY, RUSSIAN ACADEMY OF SCIENCE, RU-142432 CHERNOGOLOVKA, RUSSIA

[4]GEOLOGICAL INSTITUTE, RUSSIAN ACADEMY OF SCIENCE, RU-670047 ULAN-UDE, RUSSIA

RECEIVED MARCH 9, 2001; REVISED TYPESCRIPT ACCEPTED APRIL 24, 2002

A petrological study was carried out on Mg-skarn-bearing dunite cumulates that are part of the Neo-Proterozoic Ioko-Dovyren intrusion (North Baikal region, Russia). Skarn xenoliths contain brucite pseudomorphs after periclase, forsterite and Cr-poor spinel. Fine-grained forsterite–spinel skarns occur with the brucite skarns or as isolated schlieren. Field relationships reveal that the Mg-skarns formed from silica-poor dolomitic xenoliths by interaction with the mafic magma of the Ioko-Dovyren intrusion. Rapid heating of dolomitic xenoliths by the mafic magma caused the decomposition of dolomite into calcite + periclase, releasing much CO_2. Further heating quantitatively melted the calcite. A periclase-rich restite was left behind after extraction of the low-density, low-viscosity calcite melt. The extracted calcite melt mixed with the surrounding mafic melt. This resulted in crystallization of olivine with CaO contents up to 1·67 wt %. A local decrease in the silica concentration stabilized $CaAl_2SiO_6$-rich clinopyroxene. Brucite/periclase-free forsterite–spinel skarns probably originated by crystallization from the mafic melt close to the xenoliths at elevated fO_2. The high fO_2 was caused by CO_2-rich fluids released during the decomposition of the xenoliths. The above case study provides the first evidence for partial melting of dolomite xenoliths during incorporation by a mafic magma.

KEY WORDS: *dunite; dolomite assimilation; partial melting*

INTRODUCTION

Chemical signatures of primitive mafic magmas are primarily determined by the source composition (i.e. enriched or depleted mantle domains) and the conditions of melt formation (e.g. fluid saturation and oxygen fugacity; see, e.g. Green & Ringwood, 1967; Lloyd & Bailey, 1975; Mysen & Boettcher, 1975). Classical examples are the 'MORB signature' of tholeiitic basalts (e.g. Sun *et al.*, 1979) and the 'subduction signature' of calc-alkaline series (e.g. Miyashiro, 1974). On the basis of modelling results (e.g. Patchett, 1980; Huppert & Sparks, 1985) and geochemical evidence (e.g. Thirlwall & Jones, 1983; Thompson *et al.*, 1984; Puchtel *et al.*, 1997), it is well established that intracontinental mafic and ultramafic magmas can experience significant crustal contamination and, therefore, modification of their original characteristics. Mineralogical and geochemical evidence for basalt contamination by silica-rich crustal material has

*Corresponding author. Present address: Institut für Mineralogie, Petrologie und Geochemie, Universität Tübingen, D-72074 Tübingen, Germany. Telephone: 0049-7071-2972602. Fax: 0049-7071-293060. E-mail: thomas.wenzel@uni-tuebingen.de

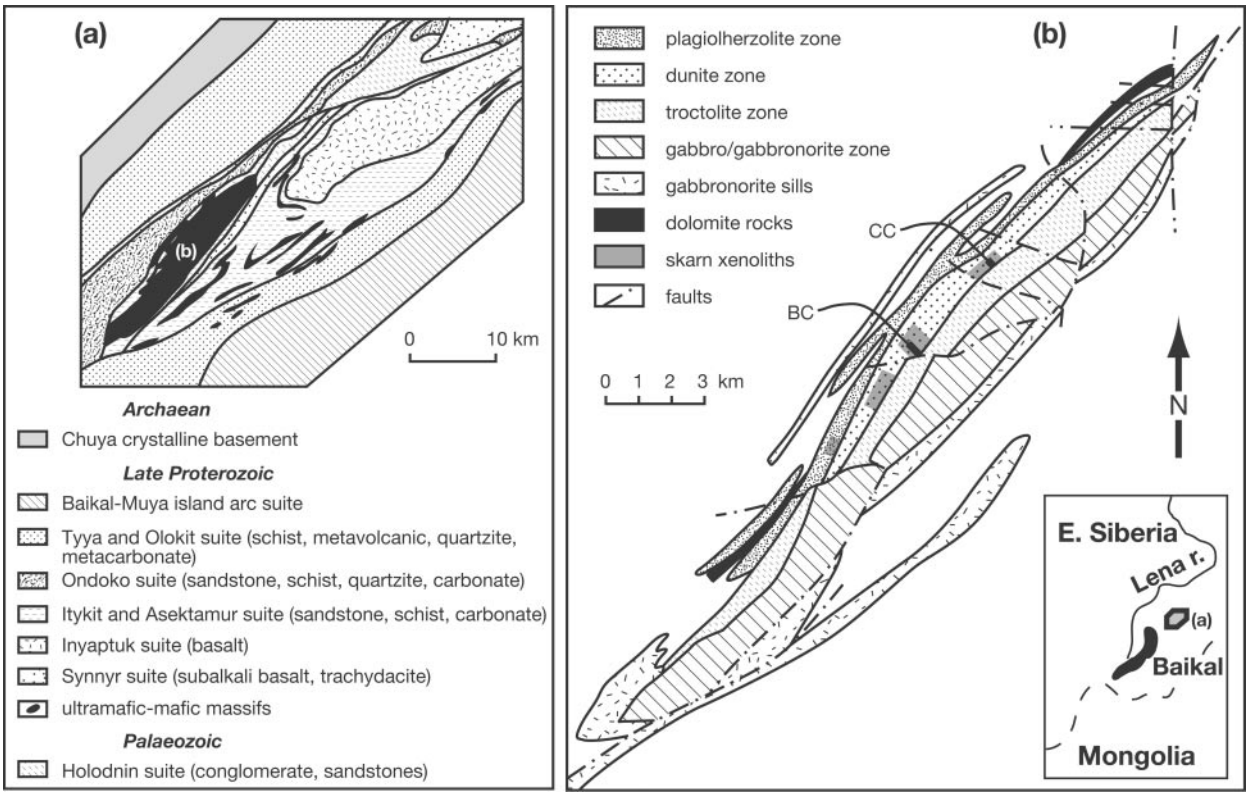

Fig. 1. Simplified geological map of (a) the Northern Baikal region and (b) the Ioko-Dovyren intrusion, modified after Konnikov *et al.* (1994); black bars, locations of the sections through the dunite zone; BC, Bol'schoi Creek; CC, Central Creek. Outcrops in which Mg-skarn xenoliths were observed are marked as grey fields in (b).

been detected in many zoned plutons and layered intrusions (e.g. Gray *et al.*, 1981; Stewart & DePaolo, 1992; Francis, 1994; Reiners *et al.*, 1996; Tegner *et al.*, 1999; Maier *et al.*, 2000). Layered intrusions are particularly suitable objects for such investigations because they provide detailed insight into the evolutionary processes of crustal magma chambers (e.g. Turner & Campbell, 1986).

In the early days of igneous petrology, carbonate assimilation was a popular model to explain variations in the composition of mafic magmas, in particular in the context of the origin of alkaline rocks (e.g. Daly, 1910; Shand, 1930). Modern studies of the trace element and isotope compositions of alkaline igneous rocks and mantle xenoliths indicate that this model is untenable. However, several studies dealing with limestone assimilation by mafic magma (e.g. Tilley, 1952; Joesten, 1977; Baker & Black, 1980; Joesten *et al.*, 1994; Owens, 2000) noted major changes in the chemical composition and mineralogy of the mafic magma, such as the resorption of primary igneous minerals (e.g. olivine, clinopyroxene), and the crystallization of Ca–Al-rich clinopyroxene, wollastonite and nepheline. Calc-silicate minerals such as wollastonite, andradite, grossular, spurrite, rankinite, merwinite and melilite were described as having formed at the magma–limestone interface. Actual melting of calcite has never been observed.

In this paper, we present the results of detailed petrological investigations of Mg-skarn-bearing dunites that are part of the Neo-Proterozoic Ioko-Dovyren intrusion. On the basis of geochemical data, model calculations and published experimental results, we provide evidence for (1) the metamorphic transformation of dolomite xenoliths to Ca-free Mg-skarns by quantitative extraction of a calcite melt, (2) the mixing of the calcite melt with the mafic magma, and (3) the effect of CO_2 produced by metamorphic breakdown reactions of the xenolith assemblages on the chemical equilibrium between mafic magma and crystallizing minerals.

GEOLOGICAL SETTING

The Ioko-Dovyren layered intrusion is situated at the southeastern margin of the East Siberian platform within the Olokit trough (e.g. Konnikov *et al.*, 1994; Fig. 1a). Low-grade Neo-Proterozoic sandstones, schists and carbonates of the Ondoko, Itykit and Asektamur suites were

intruded. The metasediments are overlain by basic to intermediate, tholeiitic volcanic rocks belonging to the Inyaptuk and Synnyr suites. Similar ages, 700 ± 20 Ma (U–Pb zircon) for tholeiitic basalts (Neimark *et al.*, 1991) and 673 ± 22 Ma (Sm/Nd whole rock) for gabbros of the Ioko-Dovyren intrusion (Amelin *et al.*, 1996), have been interpreted to be the result of a cogenetic relationship of the effusive and the intrusive series (e.g. Konnikov *et al.*, 1994; Kislov, 1998).

The Ioko-Dovyren intrusion is about 26 km long and has a thickness of roughly 3·5 km. It is composed of four zones named after the dominant cumulate rock types. From bottom to top these are the plagiolherzolite zone, dunite zone, troctolite zone and gabbro–gabbronorite zone (Fig. 1b; Konnikov *et al.*, 1994). Granophyric gabbronorites form a belt of sills and dykes below and above the intrusion. The subvertical dip of the magmatic layering of the intrusives is concordant with bedding in the enclosing metasedimentary country rocks and is the result of a post-intrusive, regional tectonism at ~550 Ma [see Amelin *et al.* (1996) for discussion].

Xenoliths of Mg-rich skarns ranging from a few centimetres to 20 m in size are widespread in the dunite zone (Fig. 1b). Two types of skarns were observed (Pertzev & Shabynin, 1979): the first is composed of brucite, olivine and spinel without Ca-bearing minerals; the second is composed of olivine and spinel, sometimes including monticellite and diopside. Pressures between 0·5 and 1·5 kbar have been proposed for monticellite-bearing skarn assemblages (Alexandrov, 1990). Efimov *et al.* (1986) observed high-temperature melilite–olivine–Ti-fassaite–perovskite associations in calc-silicate xenoliths from the troctolite zone, and calculated a pressure of <1·5 kbar. A minimum pressure of ~1 kbar is indicated by the thickness of ~3·5 km of the Ioko-Dovyren intrusion.

SAMPLING AND ANALYTICAL PROCEDURES

A total of 105 igneous rock samples of the Ioko-Dovyren intrusion and 72 samples of typical country rocks and skarn xenoliths were collected during a field trip in 1999. Thirty-eight dunite samples and 13 skarn xenoliths from two sections through the upper 450–500 m of the dunite zone were selected for detailed mineralogical and geochemical investigations. Mg-rich skarn xenoliths are concentrated in this part of the dunite zone. The sections are located in the 'Central Creek' (hereafter CC) and 'Bol'schoi Creek' (hereafter BC; see Fig. 1b) where continuous outcrops are present. The transition between the dunite and the troctolite zone is preserved in the CC section, whereas it is cut by a shear zone in the BC section. Hence, correlation based on igneous stratigraphy is approximate.

Polished thin sections were used for the petrographical description of the rocks and for microprobe analyses. Analyses were performed with a JEOL JXA 8900 RL-Superprobe at the University of Mainz, using a 20 kV acceleration voltage and a 20 nA beam current for olivine and spinel, and 15 kV and 12 nA for clinopyroxene and plagioclase. Natural minerals (albite, haematite, olivine, orthoclase, rhodonite, wollastonite) and high-purity oxides (corundum, Cr_2O_3, NiO, periclase, rutile) and metals (Zn) were used for standardization. The PhiRhoZet program of JEOL was used for data reduction. Up to 35 individual analyses of each type of mineral were made for each thin section. A few samples were strongly altered. In these rare cases, only 1–2 analyses of fresh mineral relics were made.

Major and trace element compositions of whole-rock samples were determined by X-ray fluorescence (XRF) using a Philips PW 1404 X-ray spectrometer at the University of Mainz. Reproducibility is better than 0·4% relative for major elements, based on comparison with results of reference samples and on duplicate analyses. Relative deviations between measured and recommended trace element concentrations of international standards range from 1 to 10% [see Wenzel *et al.* (1997) for details]. Carbon and sulphur were determined using a LECO CS-225 IR apparatus, with a reproducibility better than ±0·5% for C and ±5% for S. Loss on ignition (LOI) was determined gravimetrically at 1000°C. The analytical precision is better than 5%.

RESULTS AND INTERPRETATION

Petrography

Dunitic cumulates

The dunite zone is composed of dunites, plagiodunites and wehrlites. Samples taken away from skarn xenoliths contain olivine and spinel as cumulus minerals, and plagioclase and clinopyroxene as intercumulus minerals. Textures indicate a crystallization sequence of spinel followed by olivine, then plagioclase and finally clinopyroxene. Intercumulus plagioclase is generally absent in and just above the skarn-bearing horizons, whereas poikilitic clinopyroxene is concentrated at these levels. Anhedral Fe–Ni–Cu sulphides are frequently observed in samples from the upper part of the sections. They often have irregular rims of magnetite and haematite. The samples from the dunite zone are ortho-, meso- and adcumulates according to the criteria of Irvine (1982) (Table 1). There are obvious variations in the textural characteristics even on the scale of a thin section. Parts with cumulus minerals enclosed by intercumulus phases occur together with parts that show adcumulate textures

Table 1: Petrography of igneous samples from the CC and BC sections

Sample number	Sample position (m)	Cumulus minerals	Intercumulus minerals	Abundance of intercumulus	Type of cumulate (Irvine, 1982)
CC section					
99-DV38	0	Spl, Ol	Pl, Cpx	14	meso
99-DV39	4	Spl?, Ol		<1	ad
99-DV40	12	Spl, Ol	Pl, Cpx	20	meso
99-DV41	16	Spl, Ol		<1	ad
99-DV42	36	Spl?, Ol		<1	ad
99-DV43	48	Spl?, Ol		<1	ad
99-DV44	54	Spl, Ol	Pl, Cpx	15	meso
99-DV45	66	Spl, Ol		<1	ad
99-DV46	102	Spl, Ol	Cpx	14	meso
99-DV48	144	Spl, Ol	Cpx	19	meso
99-DV49	172	Spl, Ol	Cpx	<3	ad
99-DV50	202	Spl?, Ol		<1	ad
99-DV51	262	Spl?, Ol		<1	ad
99-DV52	280	Spl, Ol	Cpx	13	meso
99-DV53	306	Spl, Ol	Cpx	19	meso
99-DV55	342	Spl, Ol	Cpx	5	ad
99-DV56	358	Spl, Ol	Cpx	13	meso
99-DV57	386	Spl, Ol	Cpx	18	meso
99-DV58	414	Spl, Ol	Cpx	10	meso
99-DV59	436	Spl, Ol	Cpx	28	ortho
BC section					
99-DV105	0	Spl, Ol	Am	21	meso
99-DV103	42	Spl, Ol		<1	ad
99-DV102	88	Spl, Ol	Cpx	13	meso
99-DV101	128	Spl?, Ol		<1	ad
99-DV100	168	Spl?, Ol		<1	ad
99-DV99	180	Spl, Ol	Cpx	<3	ad
99-DV97	228	Spl, Ol	Cpx	7	meso
99-DV95	280	Spl, Ol	Cpx	31	ortho
99-DV93	308	Spl, Ol	Cpx	35	ortho
99-DV92	312	Spl, Ol	Cpx	<3	ad
99-DV91	316	Spl?, Ol		<1	ad
99-DV89	340	Spl, Ol	Cpx	16	meso
99-DV86	348	Spl?, Ol		<1	ad
99-DV84	352	Spl, Ol	Cpx	50	ortho
99-DV83	362	Spl, Ol	Cpx	49	ortho
99-DV82	392	Spl, Ol	Cpx	30	ortho
99-DV81	404	Spl, Ol	Cpx	16	meso

The abundance of intercumulus minerals was determined using thin sections. The origin of spinel is uncertain (?) in samples that are totally recrystallized. ortho, orthocumulate; meso, mesocumulate, ad, adcumulate. Sample position is in metres above the base of the section.

Table 2: Typical olivine compositions (wt %) determined by electron microprobe

Sample:	99-DV44	99-DV44	99-DV51	99-DV51	99-DV93	99-DV93	99-DV38x	99-DV47
SiO_2	40·44	40·31	40·73	40·83	40·73	41·02	42·44	42·10
Al_2O_3	0·00	0·01	0·03	0·02	0·01	0·03	0·03	0·05
Cr_2O_3	0·03	0·05	0·03	0·04	0·04	0·04	0·02	0·09
FeO	11·98	12·00	9·62	9·43	7·60	7·79	1·29	1·58
NiO	0·23	0·25	0·11	0·11	0·11	0·12	0·01	0·04
MgO	47·39	47·21	48·70	48·99	50·10	49·88	55·37	55·54
CaO	0·05	0·06	0·67	0·63	0·60	0·64	1·00	0·28
MnO	0·19	0·21	0·17	0·17	0·16	0·16	0·08	0·12
Total	100·31	100·10	100·06	100·21	99·35	99·68	100·23	99·81
Formula								
Si	0·999	0·998	0·999	0·999	0·997	1·001	1·000	0·997
Al	0·000	0·000	0·001	0·001	0·000	0·001	0·001	0·001
Cr	0·001	0·001	0·001	0·001	0·001	0·001	0·000	0·002
Fe	0·247	0·248	0·197	0·193	0·156	0·159	0·025	0·031
Ni	0·005	0·005	0·002	0·002	0·002	0·002	0·000	0·001
Mg	1·745	1·743	1·780	1·786	1·828	1·814	1·945	1·960
Ca	0·001	0·002	0·018	0·016	0·016	0·017	0·025	0·007
Mn	0·004	0·004	0·003	0·004	0·003	0·003	0·002	0·002
mg-no.	87·6	87·5	90·0	90·3	92·2	91·9	98·7	98·4
fe-no.	12·4	12·5	10·0	9·7	7·8	8·1	1·3	1·6

99-DV44, uncontaminated dunite; 99-DV51, contaminated dunite; 99-DV93, dunite close to a Mg-skarn; 99-DV38x, brucite/periclase skarn; 99-DV47, forsterite–spinel skarn. The formula was calculated on the basis of four oxygens; *mg*-number = 100Mg/(Mg + Fe), *fe*-number = 100Fe/(Mg + Fe).

with equilibrated grain boundaries. Mineral compositions of a typical skarn-free dunite, a skarn-bearing dunite (in the following, 'uncontaminated' and 'contaminated dunite'), and a dunite close to skarn xenoliths (<1 m) are given in Tables 2–5.

Skarn xenoliths

Skarn xenoliths occur in two separate horizons in the CC section, whereas they are found in the whole BC section. There are two types of skarns with different mineralogical compositions and textural relationships. Local contacts between the two skarn types are sharp. The first type is dominated by coarse-grained aggregates (>0·8 mm) of brucite with onion-skin structure (Fig. 2a). These aggregates are pseudomorphs after periclase. Anhedral to subhedral olivine and spinel fill triple junctions between the periclase pseudomorphs (Fig. 2a). The second skarn type occurs as rims on brucite-rich skarns and as isolated schlieren-like bodies within the dunitic cumulate. The schlieren often exhibit an almost vertical orientation (Gurulev, 1983). They are composed of fine-grained (<0·2 mm) olivine and spinel (Fig. 2b). The fine-grained skarns are locally intruded by veins or intercalated with layers (<2 mm thickness) containing coarse-grained olivine and spinel. Poikilitic monticellite enclosing olivine and spinel was observed in skarn schlieren from the BC section (Fig. 2c). Back-scattered electron images revealed that monticellite is locally intergrown with sub-microscopic clinopyroxene. Some of the olivine–spinel skarns contain small (<0·2 mm) grains of pentlandite surrounded by irregular rims of chalcopyrite. Calcite occurs only in veins cutting the skarns and dunites. These veins are clearly of late-stage, low-temperature origin. Mineral compositions of both skarn types are presented in Tables 2 and 3.

Whole-rock chemistry

Dunitic cumulates

The major element composition of the dunite samples (Table 6) essentially reflects the accumulation of olivine. Most major and trace elements show only small variation along the CC and BC sections. Cu is well correlated with the sulphur content of the dunite samples (not shown) and reflects the distribution of sulphide minerals.

Table 3: Typical spinel compositions (wt %) determined by electron microprobe

Sample:	99-DV44	99-DV44	99-DV51	99-DV51	99-DV93	99-DV93	99-DV38x	99-DV47
SiO_2	0·40	0·38	0·01	0·00	0·05	0·06	0·04	0·07
TiO_2	1·80	2·36	0·30	0·57	0·15	0·13	0·55	0·28
Al_2O_3	14·77	15·66	37·97	34·84	51·33	51·35	56·64	47·63
Cr_2O_3	41·97	41·01	18·22	15·62	12·70	12·39	0·06	7·59
FeO	32·16	30·59	27·60	34·63	12·30	12·76	15·47	19·35
MnO	0·32	0·29	0·21	0·33	0·11	0·07	0·02	0·17
MgO	7·61	8·86	15·57	13·91	20·10	20·02	26·00	24·69
ZnO	0·21	0·21	0·17	0·16	0·11	0·10	0·03	0·06
Total	99·24	99·36	100·05	100·06	96·86	96·88	98·81	99·85
Formula								
Si	0·013	0·012	0·000	0·000	0·001	0·002	0·001	0·002
Ti	0·045	0·058	0·006	0·012	0·003	0·003	0·010	0·006
Al	0·574	0·600	1·267	1·185	1·633	1·634	1·683	1·457
Cr	1·094	1·055	0·408	0·356	0·271	0·264	0·001	0·156
Fe III	0·217	0·205	0·312	0·433	0·087	0·093	0·293	0·373
Fe II	0·670	0·627	0·341	0·402	0·191	0·195	0·033	0·047
Mn	0·009	0·008	0·005	0·008	0·002	0·002	0·001	0·004
Mg	0·374	0·430	0·657	0·599	0·809	0·806	0·977	0·955
Zn	0·005	0·005	0·004	0·003	0·002	0·002	0·001	0·001
cr-no.	65·6	63·7	24·4	23·1	14·2	13·9	0·1	9·7
mg-no.	35·8	40·7	65·8	59·8	80·9	80·5	96·7	95·3

99-DV44, uncontaminated dunite; 99-DV51, contaminated dunite; 99-DV93, dunite close to a Mg-skarn; 99-DV38x, brucite/periclase skarn; 99-DV47, forsterite–spinel skarn. The formula was calculated on the basis of three cations (Droop, 1987); *cr*-number = 100Cr/(Cr + Al); *mg*-number = 100Mg/(Mg + Fe^{II}).

The variation of CaO and Sr (Fig. 3) can be theoretically used as an indicator of carbonate contamination. However, plots of CaO vs MgO and Sr vs the modal content of intercumulus minerals show that these compositional variations are mainly related to the varying content of intercumulus plagioclase and clinopyroxene (Fig. 3).

Skarn xenoliths

Periclase–forsterite–spinel skarns are very rich in MgO (>53·6 wt %; see Table 7). MgO varies between 66 and 81 wt % on an anhydrous basis. Periclase skarns have low concentrations of SiO_2 (2·9–14·2 wt %), Al_2O_3 (1·2–4·3 wt %) and Fe_2O_3 (5·7–9·4 wt %). Na_2O and K_2O concentrations are below the detection limit (<0·01 wt %) for most samples. The periclase skarns are almost CaO free (<0·3 wt %). Trace element concentrations of periclase skarns are at low levels (Table 7), except for two samples that show elevated Co (>194 ppm), Ni (>1522 ppm) and Cu (>165 ppm) concentrations.

The major element composition of fine-grained olivine–spinel skarns (Table 7) is dominated by MgO (41·5–49·5 wt %), SiO_2 (35·3–32·3 wt %) and Al_2O_3 (9·2–9·7 wt %). Na_2O, K_2O and CaO are close to or below the detection limit. Monticellite-bearing skarns are enriched in CaO and contain up to 21 wt % CaO. The concentrations of Rb, Sr, Y, Zr, Nb and Ba are very low in these skarns, whereas Cr ranges between 73 and 550 ppm, and Ni between 32 and 910 ppm. One sample is anomalously high in Ni (>2602 ppm) and Co (>168 ppm). The Ni, Co and Cu enrichment of some skarns is most probably related to the presence of sulphides that have been detected by electron microprobe studies.

Mineral chemistry of dunites

Spinel

Spinels enclosed by cumulus olivine show a large variability in *cr*-number [100Cr/(Cr + Al) in mol %] from 24 to 71 in rocks from the CC section (Fig. 4a) and from

Table 4: Typical clinopyroxene compositions (wt %) determined by electron microprobe

Sample:	99-DV44	99-DV44	99-DV83	99-DV83	99-DV83
SiO_2	52·57	52·64	49·31	48·40	48·47
TiO_2	0·25	0·69	0·43	0·49	0·42
Al_2O_3	2·97	2·41	6·42	7·16	6·76
Cr_2O_3	1·19	0·97	1·03	0·95	1·15
FeO	3·81	3·70	3·29	3·47	3·19
MnO	0·17	0·16	0·03	0·06	0·06
MgO	17·42	17·17	14·52	14·47	14·56
CaO	21·34	2·81	24·38	24·61	24·34
Na_2O	0·33	0·44	0·22	0·15	0·20
K_2O	0·00	0·00	0·01	0·00	0·00
Total	100·05	99·99	99·64	99·76	99·14
Formula					
Si	1·912	1·917	1·810	1·774	1·786
Ti	0·007	0·019	0·012	0·013	0·012
Al	0·127	0·103	0·278	0·309	0·294
Cr	0·034	0·028	0·030	0·027	0·034
Fe III	0·025	0·027	0·065	0·100	0·091
Fe II	0·091	0·086	0·036	0·007	0·007
Mn	0·005	0·005	0·001	0·002	0·002
Mg	0·944	0·932	0·794	0·791	0·800
Ca	0·831	0·851	0·959	0·966	0·961
Na	0·023	0·031	0·016	0·011	0·014
K	0·000	0·000	0·000	0·000	0·000
Cats	0·0055	0·0027	0·0290	0·0321	0·0294

99-DV44, uncontaminated dunite; 99-DV83, contaminated dunite. The formula was calculated on the basis of four cations (Droop, 1987). Cats, Ca-Tschermak's component.

Table 5: Typical plagioclase compositions (wt %) of uncontaminated dunite (99-DV44) determined by electron microprobe

Sample:	99-DV44	99-DV44	99-DV44	99-DV44	99-DV44
SiO_2	54·06	50·00	54·69	48·47	49·25
Al_2O_3	28·73	31·30	28·23	32·64	32·22
FeO	0·29	0·17	0·19	0·19	0·15
CaO	11·46	14·63	11·02	16·18	15·63
Na_2O	4·95	3·40	5·56	2·58	2·74
K_2O	0·30	0·17	0·18	0·12	0·18
Total	99·79	99·67	99·87	100·18	100·01
Formula					
Si	2·451	2·292	2·475	2·219	2·252
Al	1·535	1·691	1·506	1·761	1·736
Fe	0·011	0·007	0·007	0·007	0·006
Ca	0·557	0·718	0·534	0·794	0·766
Na	0·435	0·302	0·488	0·229	0·229
K	0·017	0·010	0·010	0·007	0·010
Or	1·7	1·0	1·0	0·7	1·0
Ab	43·1	29·3	47·2	22·2	22·8
An	55·2	69·7	51·7	77·1	76·2

The formula was calculated on the basis of eight oxygens. Or = K/(K + Na + Ca); Ab = Na/(K + Na + Ca); An = Ca/(K + Na + Ca).

13 to 58 in the BC section (Fig. 4b). The *mg*-number of spinel inclusions [100Mg/(Mg + Fe^{2+}) in mol %] is between 33 and 60 in CC (Fig. 4a) and between 40 and 81 in BC (Fig. 4b). High *cr*-number paired with low *mg*-number predominates within the lower 100 m of the dunite sections. Dunite samples close to skarn xenoliths contain spinel that has typically low *cr*-number (<30) and high *mg*-number (~70–80) values.

Spinel shows increasing *cr*-number with decreasing *mg*-number (Fig. 5). This trend is in contrast to the trend produced by fractional crystallization of olivine (Dick & Bullen, 1984). Fractionation of olivine and plagioclase is also excluded because plagioclase does not occur as a cumulus mineral in the dunite zone. Subsolidus hydrothermal alteration would cause a trend of increasing *cr*-number and/or decreasing *mg*-number (Kimball, 1990). However, the spinel grains analysed were enclosed by fresh olivine. The observed pattern (Fig. 5) is consistent with near-isothermal equilibration of spinel with olivine of nearly uniform composition (see Dick & Bullen, 1984). Equilibration temperatures of 18 spinel–olivine pairs from the lower, uncontaminated part of the dunite zone scatter between 754 and 794°C using the thermometer of Sack & Ghiorso (1991). These temperatures are too low for the solidus. Hence, diffusional re-equilibration at subsolidus temperatures occurred in spinel despite the fact that both olivine and spinel look pristine.

Olivine

The *mg*-number of cumulus olivine varies from 85·6 to 92·2 in the sections (Fig. 6a and b). Dunite samples collected close to skarn xenoliths contain the olivine that is most Mg rich (*mg*-number >89·5).

The NiO content of olivine varies as a function of depth (Fig. 6a and b). Both sections start with high NiO values of 0·23–0·25 wt %. Similar high NiO values were also reported in the literature for the dunite zone below the present sections (Kislov, 1998). The CC and BC sections are similar in that olivine is relatively Ni poor between ~200 and 350 m. Increasing NiO contents

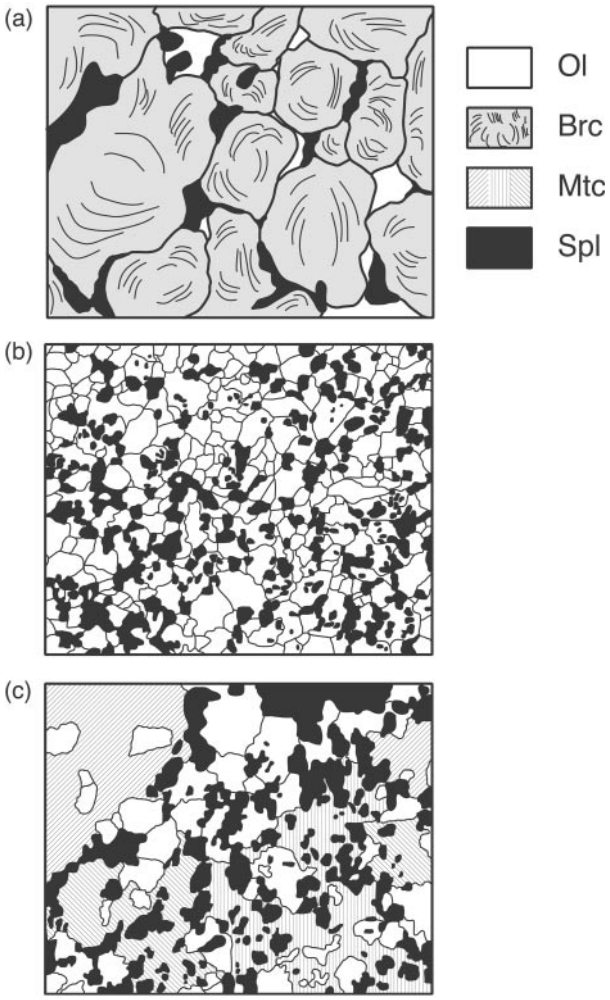

Fig. 2. Textural characteristics of (a) periclase skarns, (b) olivine–spinel skarns and (c) monticellite-bearing olivine–spinel skarns. The field of view of each figure is 2 mm.

(0·18–0·22 wt %) were observed in the upper part of the CC and BC sections. The thickness of this NiO-rich zone is larger in the CC section. The repeated increase of the NiO content of olivine is characteristic for multiple replenishment of the magma chamber (see Irvine, 1980).

Using the CaO concentrations of olivine, the CC section can be subdivided into four segments (Fig. 6a). Olivine from the lowermost 70 m of the profile contains low amounts of CaO (<0·3 wt %), which is in agreement with literature values from the lower 500 m of the dunite zone (Kislov, 1998). A first increase to 0·88 wt % is observed immediately above the first xenolith-bearing horizon. Within the following 100 m, cumulus olivine is again relatively poor in CaO (<0·3 wt %). A second increase is observed in the upper half of the second skarn-rich horizon. CaO is high (up to 1·05 wt %) in the 75 m following the skarns. Afterwards, the CaO content of olivine decreases to its initial values (<0·3 wt %). Characteristically, CaO-enriched olivines are observed in zones with relatively low concentrations of NiO.

Three samples in or on top of the skarn-bearing horizons show a much larger scatter in their CaO concentrations (Fig. 6a). Here, olivine grains show patches of CaO-poor and CaO-rich compositions (Fig. 7). The calcium distribution pattern observed is different from that of a regular growth zonation. It might reflect reaction of primary cumulus olivine with percolating intercumulus liquid enriched in CaO.

The CaO content of olivine of the BC section varies between 0·05 and 1·67 wt % (Fig. 6b). With the exception of the lowermost olivine grains, which are poor in CaO, the samples have generally high CaO contents. However, CaO concentrations of >0·7 wt % predominate in the upper half of the BC section. A decrease in the CaO content of olivine cannot be observed toward the dunite–troctolite transition, in contrast to the CC section. Again, some samples are characterized by irregular CaO distribution patterns (Fig. 6b).

Plagioclase

Intercumulus plagioclase was detected only in three thin sections from the lower part of the CC section. The anorthite content of different grains ranges from 93 to 42 mol %. Only a few grains show a regular growth zonation with a decreasing anorthite content from core to rim of up to 15 mol %. The observed pattern is interpreted to be the result of fractional crystallization of the interstitial liquid.

Clinopyroxene

Clinopyroxene, classified as augite and diopside (see Morimoto, 1988), is the dominant intercumulus mineral in both sections. Most of the clinopyroxenes contain >1 wt % Cr_2O_3; only a few samples show lower Cr_2O_3 concentrations. TiO_2 concentrations of clinopyroxenes are between 0·15 and 0·75 wt %. There is no systematic variation of Cr and Ti along the sections, whereas Ca and Al show clear trends.

Clinopyroxene significantly enriched in CaO (>23 wt %) occurs in the first skarn-rich horizon of CC (one sample) and above 150 m in the CC section (Fig. 8a). Clinopyroxene from the BC section is generally rich in CaO (Fig. 8b). These CaO-rich samples are also enriched in Al_2O_3 (Fig. 8a and b). Aluminium partly occurs in octahedral coordination, as the content of Al^{IV} (2 – Si, on the basis of four cations) does not follow a 1:1 line in an Al^{IV} vs Al^{tot} diagram (not shown). Ca is well correlated with Al^{IV} and with Al^{VI} (Fig. 9) indicating that Al is mainly incorporated into the cpx as calcium Tschermak's component (Cats). Uncontaminated

Table 6: Chemical composition of dunite whole rocks from the CC and BC sections

	CC section										
Sample:	99-DV38	99-DV39	99-DV40	99-DV41	99-DV42	99-DV43	99-DV44	99-DV45	99-DV46	99-DV48	99-DV49
wt %											
SiO_2	39·24	34·22	39·62	37·15	37·24	38·53	40·09	39·71	38·63	37·63	37·79
TiO_2	0·08	0·05	0·06	0·03	0·02	0·02	0·09	0·07	0·05	0·05	0·03
Al_2O_3	1·70	7·25	1·66	0·70	0·40	0·34	1·97	1·65	1·26	1·06	2·77
Fe_2O_3	13·91	10·66	13·23	14·36	12·79	12·96	12·79	13·58	12·69	14·37	14·91
MnO	0·18	0·15	0·18	0·18	0·18	0·18	0·17	0·18	0·18	0·19	0·20
MgO	42·55	43·40	44·18	42·91	43·74	44·93	42·68	43·36	42·78	41·51	39·21
CaO	0·87	0·18	1·34	0·46	0·54	0·48	1·42	1·10	1·32	1·05	1·95
Na_2O	0·11	0·00	0·04	0·00	0·01	0·00	0·15	0·11	0·01	0·00	0·00
K_2O	0·14	0·01	0·02	0·01	0·01	0·00	0·07	0·07	0·02	0·00	0·01
P_2O_5	0·02	0·00	0·00	0·00	0·00	0·00	0·03	0·01	0·00	0·01	0·00
LOI	−0·48	4·46	0·08	3·99	5·28	2·72	0·05	−0·41	2·44	4·49	1·45
Total	98·32	100·38	100·41	99·79	100·21	100·16	99·51	99·43	99·38	100·36	98·32
S	0·007	0·146	0·038	0·541	0·160	0·036	0·003	0·005	0·048	0·026	0·005
C	0·011	0·100	0·025	0·253	0·133	0·117	0·020	0·010	0·045	0·070	0·027
ppm											
V	31	46	33	32	18	16	46	27	27	24	29
Cr	2374	979	2715	3334	1351	960	3587	3648	4048	2676	3056
Co	153	80	151	137	117	146	154	156	140	152	151
Ni	1768	328	1376	1150	764	1613	1756	1766	1817	1480	1414
Cu	n.d.	2	8	167	12	n.d.	1	2	3	26	43
Zn	72	171	86	97	76	81	75	75	74	78	117
Ga	3	10	3	3	2	3	4	3	4	4	3
Rb	7	2	4	3	3	2	6	6	4	2	4
Sr	18	3	26	24	10	8	47	21	8	8	19
Y	3	1	2	2	1	2	3	3	1	2	2
Zr	13	5	8	5	4	4	9	9	6	6	5
Nb	1	2	1	2	1	1	2	2	1	2	1
Ba	60	18	93	138	19	12	66	47	23	21	25

Table 6: continued

	CC section								
Sample:	99-DV51	99-DV52	99-DV53	99-DV54	99-DV55	99-DV56	99-DV57	99-DV58	99-DV59
wt %									
SiO_2	35·88	38·82	37·78	37·30	36·72	36·89	37·04	37·40	38·29
TiO_2	0·04	0·06	0·06	0·02	0·05	0·10	0·08	0·07	0·10
Al_2O_3	1·22	1·63	1·65	0·46	1·35	1·51	1·45	1·38	1·69
Fe_2O_3	13·12	13·72	14·43	13·88	14·12	14·12	14·28	13·84	13·25
MnO	0·18	0·18	0·18	0·20	0·19	0·20	0·20	0·17	0·14
MgO	42·06	40·97	40·84	42·88	40·26	38·54	41·33	40·22	37·55
CaO	0·75	2·71	2·24	0·96	1·64	2·27	1·43	0·98	2·94
Na_2O	0·00	0·03	0·00	0·05	0·00	0·01	0·00	0·00	0·02
K_2O	0·03	0·03	0·02	0·01	0·01	0·02	0·01	0·01	0·00
P_2O_5	0·01	0·01	0·00	0·00	0·01	0·01	0·00	0·01	0·01
LOI	6·17	1·23	2·11	4·44	5·00	5·93	3·56	5·84	5·87
Total	99·46	99·39	99·31	100·20	99·35	99·60	99·38	99·92	99·86
S	1·043	0·259	0·491	0·066	0·552	0·481	0·230	0·091	0·121
C	0·115	0·142	0·054	0·128	0·078	0·118	0·226	0·071	0·060
	ppm								
V	21	32	29	13	30	44	33	33	39
Cr	2382	2130	3263	1118	3315	3210	3028	3353	3231
Co	145	133	159	141	166	157	158	142	128
Ni	1669	1751	1280	1107	2054	2005	2059	1386	1382
Cu	786	134	395	5	437	191	102	18	179
Zn	110	74	74	77	71	95	136	77	56
Ga	4	3	4	3	4	5	4	4	4
Rb	5	4	4	3	4	4	3	3	4
Sr	7	12	11	7	8	9	28	4	6
Y	2	3	2	2	2	3	2	2	3
Zr	6	9	8	5	7	12	12	11	14
Nb	1	1	2	2	1	2	2	2	2
Ba	20	19	25	16	15	22	20	10	14

	BC section										
Sample:	99-DV81	99-DV82	99-DV83	99-DV84	99-DV86	99-DV89	99-DV91	99-DV92	99-DV93	99-DV95	99-DV97
wt %											
SiO_2	37·63	38·23	39·80	37·96	42·43	37·92	36·11	36·30	35·49	36·65	36·92
TiO_2	0·04	0·06	0·06	0·12	0·22	0·08	0·02	0·12	0·05	0·06	0·05
Al_2O_3	1·08	1·67	1·05	3·17	3·32	1·79	1·44	3·82	2·69	1·99	1·44
Fe_2O_3	12·89	12·83	10·50	11·47	7·88	11·88	9·42	9·05	9·43	12·11	13·23
MnO	0·18	0·17	0·18	0·16	0·13	0·19	0·14	0·14	0·15	0·16	0·17
MgO	41·31	40·12	42·78	35·06	30·55	39·04	43·92	38·43	41·84	41·61	41·06
CaO	1·75	2·29	2·63	5·36	11·47	3·64	1·05	4·56	1·93	2·00	1·97
Na_2O	0·00	0·00	0·00	0·00	0·04	0·03	0·00	0·01	0·00	0·00	0·01
K_2O	0·00	0·01	0·00	0·00	0·00	0·00	0·00	0·05	0·00	0·04	0·01
P_2O_5	0·00	0·00	0·00	0·00	0·00	0·01	0·00	0·01	0·00	0·01	0·00
LOI	4·81	4·79	4·35	6·38	3·29	4·47	7·94	6·38	7·00	4·87	4·57
Total	99·69	100·17	101·35	99·68	99·33	99·05	100·04	98·87	98·58	99·50	99·43
S	0·076	0·377	0·064	0·302	0·065	0·318	0·054	0·178	0·366	0·503	0·190
C	0·183	0·057	0·085	0·087	0·070	0·173	0·255	0·288	0·251	0·122	0·124
ppm											
V	21	31	21	59	70	42	18	49	25	30	24
Cr	2350	3256	787	5124	1793	2816	2048	5540	3365	3213	2652
Co	143	127	124	129	74	131	97	129	128	126	133
Ni	1416	1511	811	1268	393	1159	458	860	1304	1199	1342
Cu	43	302	24	692	107	280	11	151	435	287	101
Zn	67	70	92	149	74	130	73	102	87	77	60
Ga	3	3	2	7	5	4	3	6	4	4	2
Rb	3	3	2	3	2	3	3	6	2	4	2
Sr	6	8	9	14	17	12	7	22	10	19	6
Y	2	2	2	3	5	3	1	3	2	2	2
Zr	6	7	8	13	27	11	4	17	8	9	7
Nb	1	2	1	2	2	1	1	1	2	1	1
Ba	16	17	18	26	18	25	21	69	30	49	22

Table 6: continued

	BC section					
Sample:	99-DV99	99-DV100	99-DV101	99-DV102	99-DV103	99-DV105
wt %						
SiO_2	37·26	36·65	37·01	37·24	37·08	39·57
TiO_2	0·04	0·05	0·03	0·04	0·04	0·07
Al_2O_3	0·82	1·38	0·85	1·04	0·61	1·30
Fe_2O_3	11·69	12·95	12·62	12·66	12·36	14·24
MnO	0·17	0·16	0·17	0·18	0·17	0·19
MgO	42·69	41·48	43·32	41·66	43·13	40·97
CaO	1·49	1·37	0·75	1·65	0·53	1·69
Na_2O	0·00	0·00	0·00	0·02	0·00	0·05
K_2O	0·01	0·04	0·01	0·01	0·01	0·03
P_2O_5	0·00	0·01	0·00	0·00	0·00	0·01
LOI	5·96	5·15	5·51	5·89	6·50	1·72
Total	100·13	99·24	100·27	100·39	100·43	99·84
S	0·175	0·373	0·078	0·051	0·090	0·029
C	0·180	0·141	0·138	0·144	0·127	0·054
ppm						
V	15	27	18	21	18	36
Cr	1169	2992	2969	2108	1320	2554
Co	132	163	149	142	133	146
Ni	1593	2115	1715	1575	1240	1848
Cu	190	556	18	20	41	127
Zn	73	76	77	76	82	96
Ga	3	3	3	3	3	3
Rb	3	4	2	3	4	4
Sr	16	11	9	11	6	17
Y	2	2	2	2	2	3
Zr	6	8	5	6	8	11
Nb	2	2	1	1	1	3
Ba	102	37	22	24	19	42

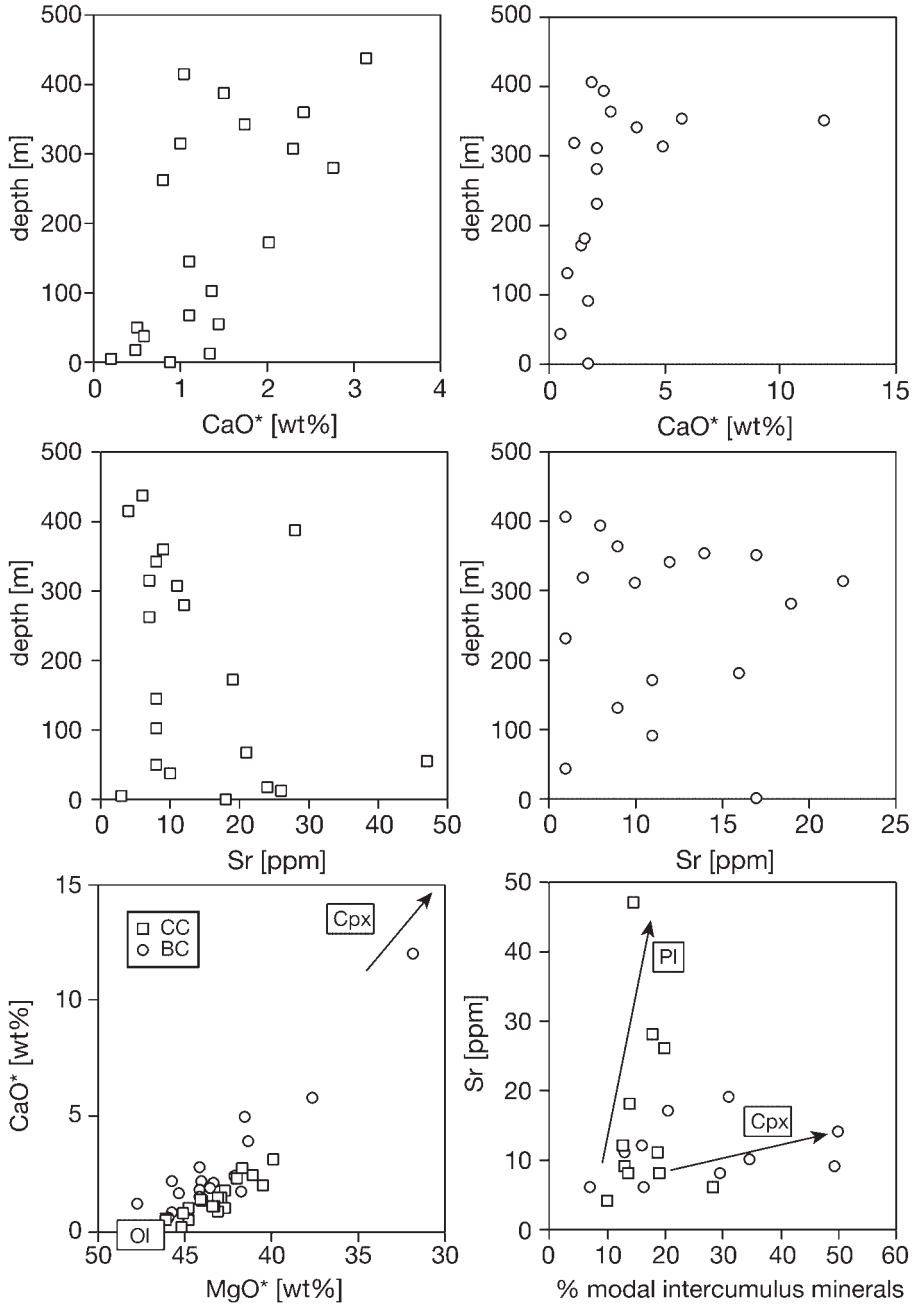

Fig. 3. The CaO*, and Sr content of dunite cumulate rocks as a function of stratigraphic height in the CC and the BC sections; *, LOI-free; sample position in metres above the base of the section. The trends shown in the plots of CaO* vs MgO* and of Sr vs modal content of intercumulus minerals indicate that the whole-rock composition is determined by the content of intercumulus plagioclase and clinopyroxene.

samples contain <0·5 mol % of Cats. The Cats content increases to 4·2 mol % in skarn-bearing dunites.

An increase in calcium in some clinopyroxenes (marked with a black star in Fig. 8a) from skarn-free dunites is, in contrast, not correlated with an aluminium increase. Ca-enriched clinopyroxenes are associated with plagioclase of relatively low anorthite content whereas clinopyroxenes with low CaO are associated with plagioclase of high An content. Therefore, the chemical variations of clinopyroxene from skarn-free dunites are probably

Table 7: Chemical composition of brucite/periclase–olivine–spinel skarns (99-DV38x, 99-DV43x, 99-DV514, 99-DV532), forsterite–spinel skarns (99-DV47, 99-DV104) and forsterite–spinel–monticellite skarns (99-DV88, 99-DV90, 99-DV94, 99-DV96)

Sample:	99-DV38x	99-DV43x	99-DV514	99-DV532	99-DV47	99-DV104	99-DV88	99-DV90	99-DV94	99-DV96
wt %										
SiO_2	2·92	14·24	3·90	10·01	25·25	32·30	37·67	30·05	7·45	26·55
TiO_2	0·04	0·13	0·03	0·17	0·34	0·27	0·02	0·25	0·15	0·24
Al_2O_3	1·35	4·32	1·16	2·82	9·24	9·70	0·49	12·51	6·22	15·19
Fe_2O_3	9·22	8·57	9·43	5·65	8·11	7·36	9·78	5·21	7·27	8·27
MnO	0·05	0·11	0·05	0·08	0·11	0·13	0·16	0·10	0·07	0·10
MgO	59·20	53·64	58·52	54·80	49·48	45·51	45·45	29·30	53·06	40·83
CaO	0·07	0·30	0·06	0·05	0·21	0·20	1·36	21·08	0·52	3·31
Na_2O	0·00	0·00	0·00	0·00	0·00	0·00	0·02	0·00	0·00	0·00
K_2O	0·01	0·00	0·00	0·00	0·01	0·00	0·01	0·01	n.d.	0·00
P_2O_5	0·00	0·00	0·00	0·00	0·01	0·00	0·00	0·02	n.d.	0·00
LOI	28·45	19·84	27·86	27·32	8·42	5·01	5·34	1·49	25·20	5·77
Total	101·24	100·85	100·95	100·85	100·97	100·28	100·30	100·02	99·94	100·26
S	0·001	0·001	0·002	0·002	0·072	0·044	0·043	n.d.	0·118	0·040
C	0·267	0·293	0·264	0·410	0·190	0·132	0·278	0·083	0·413	0·212
ppm										
V	31	27	24	12	54	28	13	53	19	70
Cr	7	90	6	19	272	348	550	73	106	397
Co	1194	91	194	24	47	25	93	20	168	79
Ni	1522	201	1814	20	228	84	383	32	2602	910
Cu	165	n.d.	204	3	6	50	14	14	11	13
Zn	71	80	69	53	53	81	62	56	39	65
Ga	3	5	2	4	10	11	1	13	5	14
Rb	3	3	2	2	2	2	3	4	2	2
Sr	n.d.	n.d.	1	1	11	5	13	51	2	4
Y	n.d.	n.d.	n.d.	7	7	9	1	17	1	6
Zr	n.d.	13	8	21	27	16	4	17	19	1
Nb	2	1	1	1	1	1	2	2	n.d.	1
Ba	13	34	13	2	21	12	25	52	6	17

n.d., below detection limit.

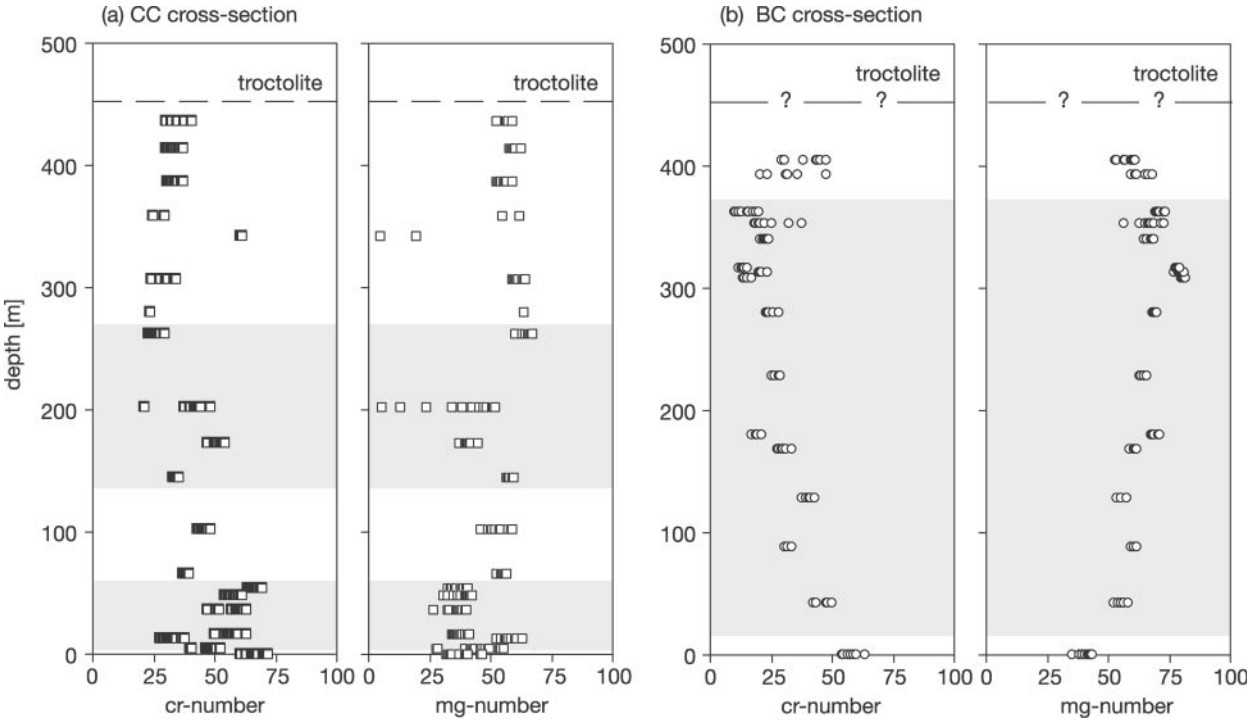

Fig. 4. Variation of *cr*-number and *mg*-number in spinel of the dunites for (a) the CC section and (b) the BC section; sample position as in Fig. 3. Grey fields indicate horizons rich in skarn xenoliths.

the result of fractional crystallization of the interstitial liquid.

Mineral chemistry of the skarn xenoliths

Spinel

Spinel in both skarn types is extremely chromium poor (*cr*-number <0·6). Its *mg*-number is very high, often >95. Iron is mostly in the ferric state according to formula calculation (Droop, 1987). Equilibration temperatures of five spinel–olivine pairs scatter between 680 and 720°C, using the calibration of Sack & Ghiorso (1991). Spinel from coarse-grained veins or layers within the fine-grained parts also shows high *mg*-number, with a tendency towards elevated *cr*-number (up to 13).

Olivine

The olivine composition in the periclase skarns is almost end-member forsterite (*mg*-number 98·1–98·9). The NiO content of this olivine is very low (<0·03 wt %), and the CaO content varies between 0·22 and 1·04 wt %. Olivine in the fine-grained olivine–spinel skarns has a similar composition (*mg*-number 98·3–98·6; NiO <0·03 wt %; CaO 0·27–0·75 wt %). Veins and coarse-grained layers within the fine-grained skarns contain forsteritic olivine, with slightly increased NiO contents (up to 0·06 wt %). This olivine is variably enriched in CaO (up to 0·56 wt %).

Monticellite

Monticellite is characterized by FeO concentrations between 1·98 and 4·09 wt % and low NiO contents (<0·06 wt %). Its composition varies in the range $Ca_{0·98–1·00}Fe_{0·08–0·10}Mg_{0·92–0·94}SiO_4$.

DISCUSSION

Composition of the parental magma of the dunite cumulates

The nature of the parental melt of the dunitic cumulates is particularly important for modelling the interaction between the magma and the skarn xenoliths. It has been repeatedly argued that the parental magma of the Ioko-Dovyren dunites was of picritic or komatiitic composition (e.g. Yaroshewskiy *et al.*, 1983; Konnikov *et al.*, 1988, 1994). This conclusion is mainly based on the weighted mean composition of the Ioko-Dovyren intrusion. However, as fractionated melts are thought to have been lost from the magma chamber by volcanic eruptions (e.g. Konnikov *et al.*, 1994), the initial concentration of elements such as Mg, which are preferentially incorporated

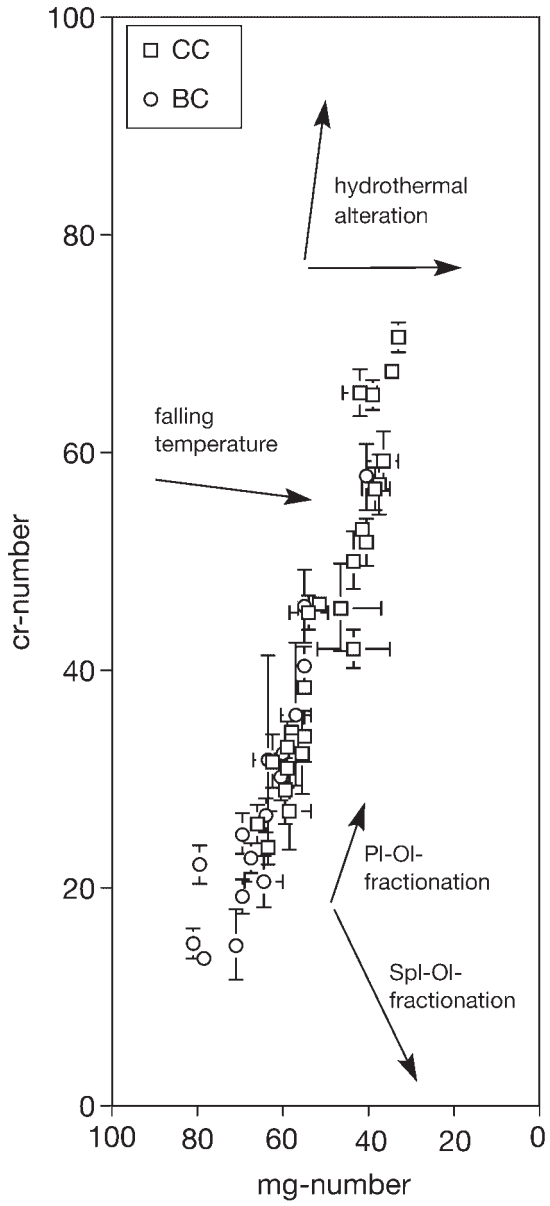

Fig. 5. Variation of *cr*-number vs *mg*-number for spinel. The mean values and standard deviations of *cr*-number and *mg*-number of spinels were calculated for every sample. Typical trends for processes that determine spinel composition (Dick & Bullen, 1984; Kimball, 1990) are shown for comparison.

by cumulus minerals, is strongly overestimated (e.g. Amelin *et al.*, 1996).

Sills and dykes of the plagiolherzolite zone have been interpreted to indicate picritic or komatiitic affinities of the Ioko-Dovyren parental magma (e.g. Konnikov *et al.*, 1994). However, these dykes also contain ~30 wt % olivine phenocrysts (Papunen *et al.*, 1992), and hence might reflect the original magmatic liquid plus a phenocryst admixture.

Additionally, Mg-rich olivine (*mg*-number >90) from the Ioko-Dovyren dunite zone has been used as an indicator for a picritic or komatiitic parental melt [see Kislov (1998) for discussion]. However, our new data do not support this hypothesis. There are separate trends of dunite olivines in an NiO vs *mg*-number diagram (Fig. 10). The first one, not well documented by the CaO-poor olivine of the CC section, is similar to the expected trend of olivine fractionation from a basaltic magma. CaO-poor olivine forms a second trend towards lower NiO contents at almost constant *mg*-number. This trend is probably produced by the segregation of an immiscible sulphide melt from the basaltic magma. Such a process removes Ni from the silicate magma and causes the crystallization of Ni-depleted olivine (see Naldrett, 1989). The third trend dominating in both sections is caused by olivine enriched in CaO. It is directed toward olivine with high *mg*-number (>90) combined with low NiO contents (<0·05 wt %). This trend is fundamentally different compared with the olivine crystallization path from a picritic or komatiitic parental melt (e.g. Cameron & Nisbet, 1982). Our interpretation of this third trend is presented below.

The MgO/FeO ratio of the parental magma has been estimated on the basis of the least fractionated, Ca-poor olivine that has been probably least affected by carbonate assimilation. This olivine (*mg*-number 86–87) was in equilibrium with magma with an *mg*-number of 66·8–64·8 assuming a distribution coefficient of 0·30 for Mg–Fe partitioning between melt and olivine (Roeder & Emslie, 1970). This olivine (NiO 0·25 wt %) was derived from a magma containing ~210 ppm Ni based on a nickel distribution coefficient of 9·5 between melt and olivine (see Hart & Davis, 1978). Thus, both *mg*-number and Ni contents are typical for basaltic melts. A basaltic parent similar to MORB was also predicted by Amelin *et al.* (1996) on the basis of trace element modelling results.

The program MELTS (Ghiorso *et al.*, 1994) was used to calculate possible crystallization temperatures of the observed minerals at a pressure of 1 kbar. Three types of mafic melts were selected for the calculation: (1) mid-ocean ridge basalt (MORB); (2) plume-type basalt; (3) calc-alkaline basalt from a destructive plate margin [composition data from Wilson (1989)]. A sequence of crystallization similar to that observed in the Ioko-Dovyren intrusion (Spl → Ol → Pl → Cpx) is typical for tholeiitic basalts such as MORB. A magma with 9·7 wt % MgO would crystallize spinel (*mg*-number ~71, *cr*-number ~43) at ~1260°C, followed by olivine (*mg*-number ~86) at ~1230°C, plagioclase (~79 mol % anorthite) at ~1200°C and clinopyroxene (~48 mol % diopside) at ~1180°C. These mineral compositions agree well with our observations, except for the *mg*-number of spinel (Table 3), which has probably been affected by diffusional

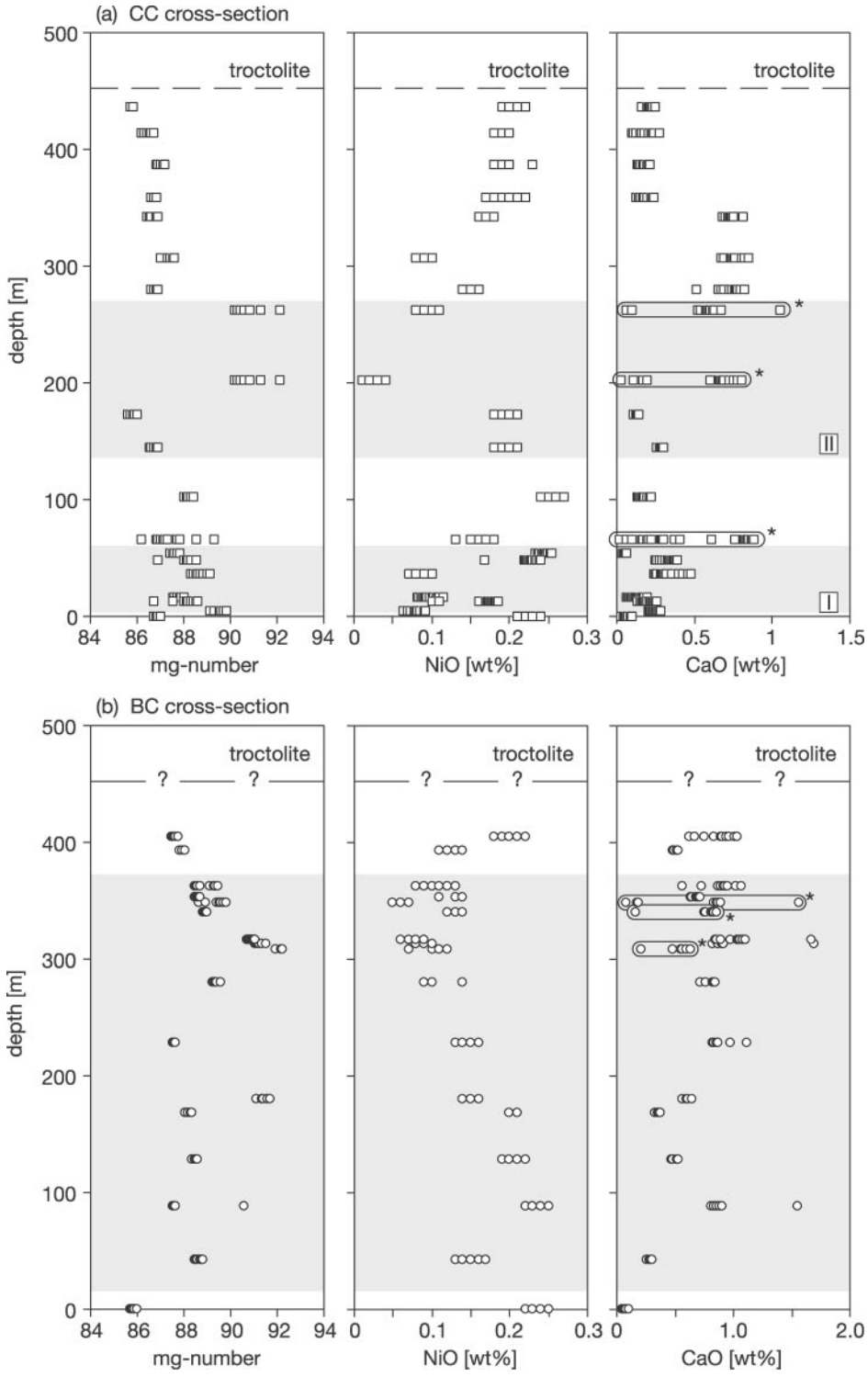

Fig. 6. The variation of *mg*-number, and the content of NiO and CaO in olivine of the dunites plotted against the sample position in (a) the CC section and (b) the BC section. Grey fields indicate horizons rich in skarn xenoliths. Samples marked with a black star are characterized by large variations of CaO contents (see Fig. 7 and text for discussion).

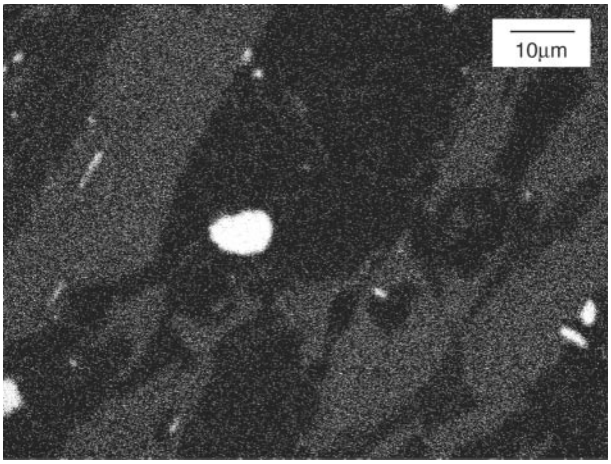

Fig. 7. X-ray map of olivine (sample 99-DV45) showing the heterogeneous distribution of Ca. Dark areas are Ca-poor olivine (<0·3 wt % CaO); grey, Ca-rich olivine (>0·5 wt % CaO); white, clinopyroxene.

sub-solidus re-equilibration (see above). Although the *cr*-number of the model spinel is not re-equilibrated, it strongly depends on the Cr content of the original magma, which is unknown for the parental melt of the Ioko-Dovyren intrusion. On the basis of the modelling results, we conclude that the dunitic cumulates of the Ioko-Dovyren intrusion crystallized in the temperature interval between about 1260 and 1180°C, assuming a pressure of 1 kbar.

Metamorphic evolution of dolomite xenoliths

Previous hypotheses for the skarn formation

The skarn xenoliths observed in the dunite zone are rich in Mg and poor in Ca. Therefore, Pertzev & Shabynin (1979) excluded dolomitic country rocks as suitable precursors for the Mg-skarns. Pertzev & Shabynin (1979) discussed two models for the formation of such skarns, both based on the high-temperature metamorphism of originally magnesite- and brucite-rich rocks. The first model assumed that the carbonate host rocks of the Ioko-Dovyren intrusion contained lens-like magnesite or brucite bodies. This is very unlikely because significant occurrences of such rocks are not known in this area (Gurulev, 1983). The second model suggests a two-stage intrusion of the Ioko-Dovyren massif. Ultramafic cumulates that formed during a first intrusive stage were subsequently hydrothermally altered to brucite or magnesite. In a second step, these were metamorphosed

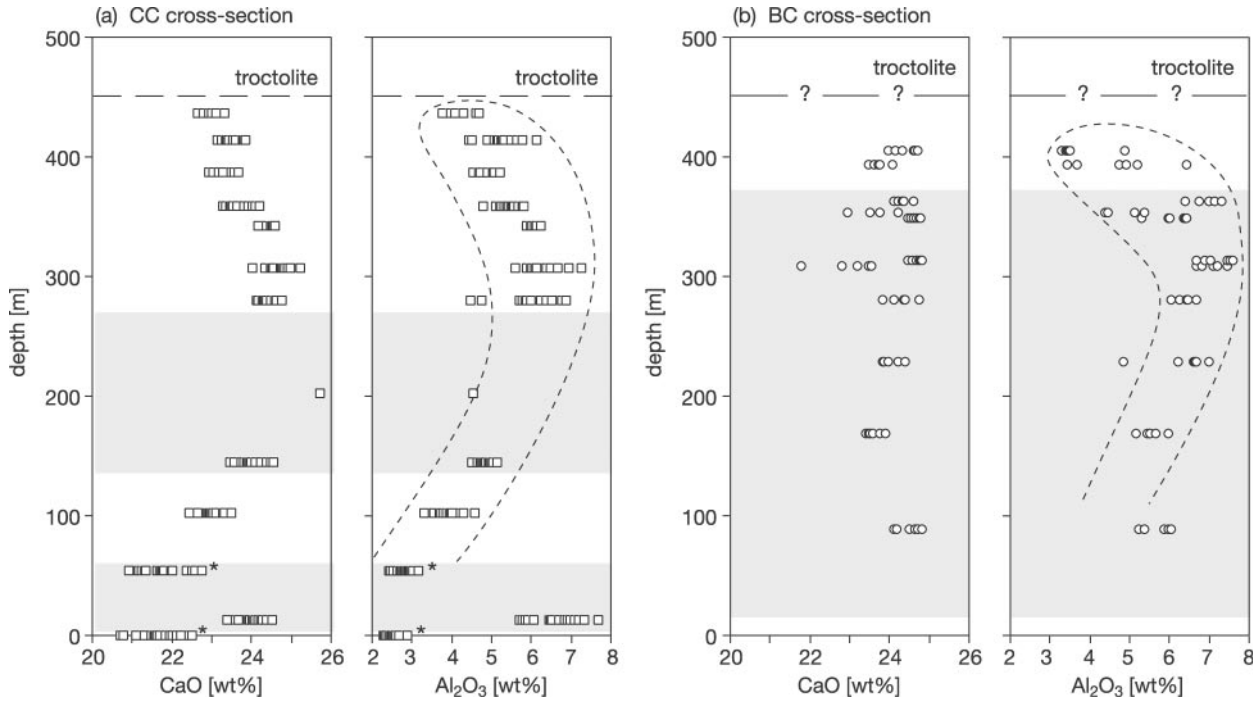

Fig. 8. Variation of CaO and Al_2O_3 content of clinopyroxene in the dunites in (a) the CC section and (b) the BC sections; sample position as in Fig. 3. Grey fields indicate horizons rich in skarn xenoliths. Uncontaminated samples marked with a black star show large variation of CaO at relatively uniform Al_2O_3 interpreted to result from fractional crystallization (see text).

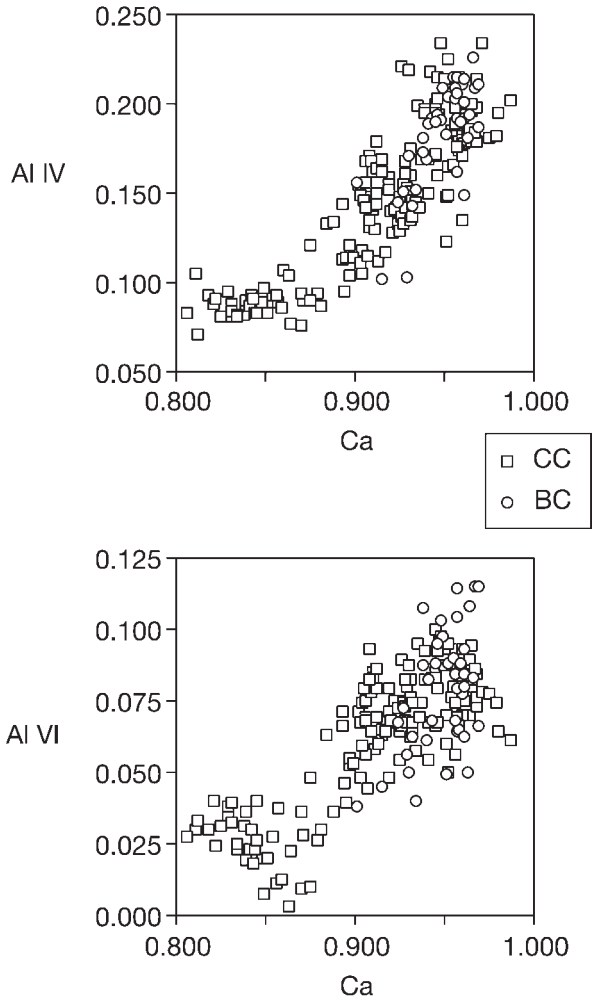

Fig. 9. Tetrahedral Al (Al IV) and octahedral Al (Al VI) plotted against Ca (cations p.f.u.) for intercumulus clinopyroxene. The collinear variation indicates incorporation of Ca-Tschermak's component (see text).

to periclase skarns during the interaction with another magma pulse. The Ioko-Dovyren intrusion clearly formed by the influx of several batches of magma. This is indicated by the spatial variations of the NiO in olivine (Fig. 6). Nevertheless, no structural or other geological evidence was found that would indicate large time gaps between distinct pulses of magma. All dunites show a similar small degree of alteration throughout the entire profile. This does not support a hydrothermal alteration between different magma pulses. It is thus unlikely that the intrusive gap lasted long enough to allow for cooling and hydrothermal alteration of a first magma pulse.

Gurulev (1983) suggested that dolomite host rocks were altered by a hydrothermal system of an early Ioko-Dovyren intrusive pulse to brucite- and serpentine-rich rocks. Subsequent pulses of magma transformed them into periclase-rich skarns. Again, no field evidence for such a contact–hydrothermal alteration process was found.

Transformation of silica-poor dolomite xenoliths to Ca-free brucite/periclase skarns

The cumulate horizons containing the Mg-skarns can be traced to dolomite layers at the margin of the intrusion (Fig. 1b). Hence, it is very likely that dolomite indeed was the protolith of the Mg-skarn xenoliths. The silica-poor dolomite host rocks consist of dolomite (>87 wt %), some calcite (<5 wt %), and detrital quartz and sheet silicates (Gurulev, 1983). The major problem is how to transform these Ca-rich rocks into virtually Ca-free rocks, composed entirely of brucite after periclase, forsterite and spinel.

A T–$X(CO_2)$ diagram was calculated for a pressure of 1 kbar using the PerPleX program (Connolly, 1990) for the MgO–CaO–SiO_2–H_2O–CO_2 system with excess calcite (Fig. 11). A quartz-poor protolith, typical for the host-rock dolomites, was assumed. In these rocks, quartz will be consumed during reaction with dolomite and water at low temperature, resulting in the formation of minor amounts of calcite + tremolite in a dolomite matrix. Tremolite will react out, producing the assemblage forsterite + calcite at a temperature below 570°C. The remaining dolomite will decompose to calcite + periclase + CO_2 at temperatures between 620 and 800°C, depending on the composition of the fluid phase. Metamorphic carbon dioxide will lead to increasing $X(CO_2)$ of the fluid phase, which will escape from the xenoliths into the surrounding magma. At 1200°C, which is the temperature at which plagioclase would form, calcite will melt even with little H_2O present [$X(CO_2)$ >0·6; Fig. 11]. As our modelling results indicate a magma temperature of at least 1260°C, it is indeed possible to completely melt the calcite in the xenolith.

The time that is necessary to heat a 1 m dolomite sphere to 700°C assuming a temperature of the mafic magma of 1200°C and a thermal diffusivity of 10^{-6} m^2/s for dolomite (Carslaw & Jaeger, 1959) is <2 days. About 5 days are required to reach 1100–1200°C. Compared with the lifetime of about 10^4-10^5 years of a mafic plutonic system (e.g. Stewart & DePaolo, 1992), there was ample time available to complete the metamorphism of the dolomite xenoliths and to melt the calcite.

Calcite melt has a low density of about 2000 kg/m^3 and a low viscosity of about 10^{-3} Pa s under the P–T conditions considered in our case (Genge *et al.*, 1995). Hence, calcite melt can be squeezed out of the xenolith by gravitational compaction caused by either the surrounding mafic magma or the dunitic crystal mush.

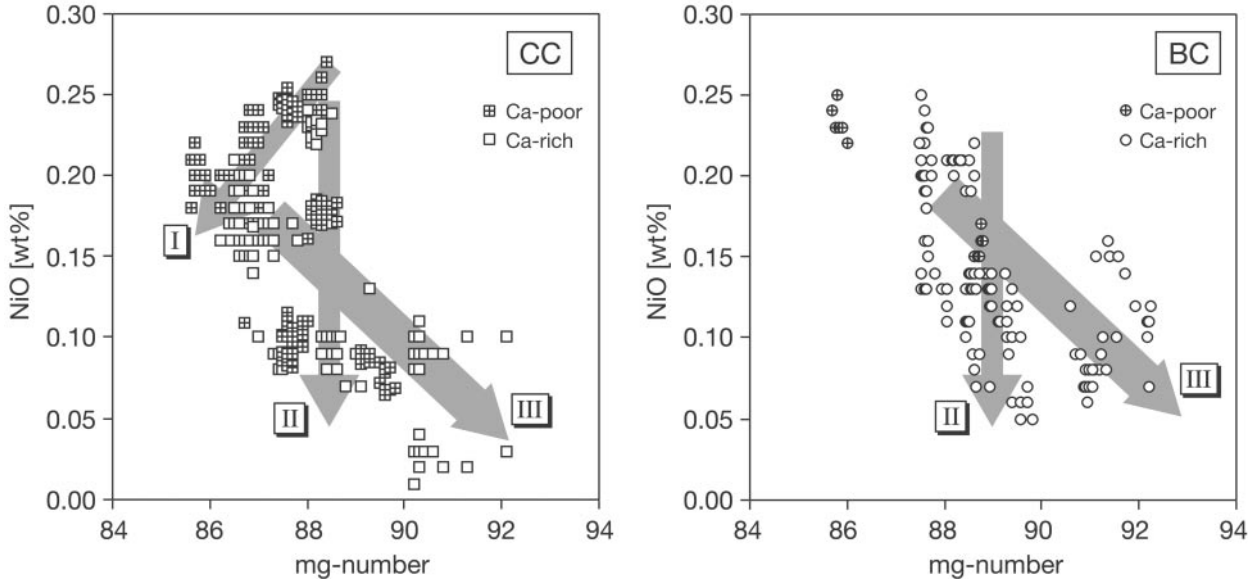

Fig. 10. NiO content of olivine vs *mg*-number for the CC and BC sections. Crossed squares, Ca-poor olivine (<0·3 wt % CaO); open squares, Ca-rich olivine (>0·3 wt % CaO). Trend I reflects fractional crystallization of olivine, trend II olivine fractionation combined with segregation of a sulphide liquid, and trend III olivine crystallization affected by high fO_2 as a result of skarn assimilation (see text).

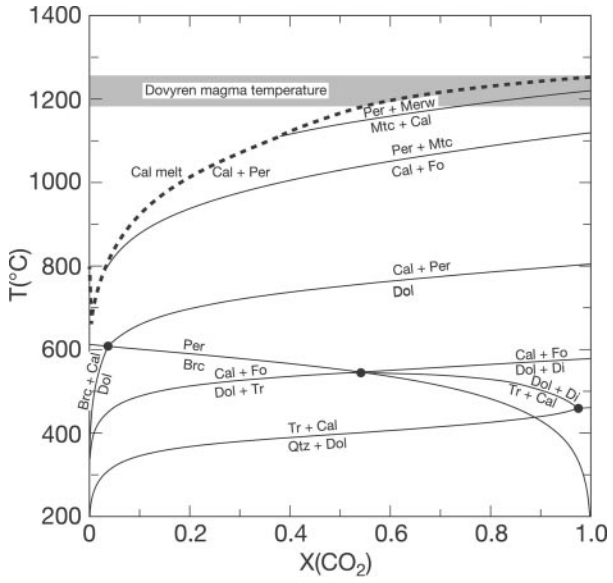

Fig. 11. Temperature vs $X(CO_2)$ diagram for the system MgO–CaO–SiO_2–H_2O–CO_2, assuming excess calcite and $P_{fluid} = P_{solid} = 1$ kbar. The PerPleX software package (Connolly, 1990) and the Holland & Powell (1998) mineral data were used for the solid–fluid reactions. The melting curve of calcite was interpolated from experimental results of Wyllie (1965). The field for the probable magma temperature is based on the modelling results using the program MELTS (Ghiorso *et al.*, 1994).

Decomposition of dolomite and the quantitative removal of calcite melt result in a volume reduction of ~70%, and a nearly Ca-free, periclase-rich restite.

Anhedral olivine and spinel fill the triple junctions between brucite pseudomorphs of periclase (Fig. 2a). This could indicate that these minerals crystallized from a silicate mafic melt, or that they recrystallized in contact with a melt. However, skarn olivine and spinel cannot simply be derived from the crystallization of the mafic magma. Olivine is distinctly more enriched in MgO and more depleted in NiO compared with olivine of the dunites. Skarn spinel is almost Cr free, in contrast to the Cr-rich spinel observed in the dunites.

Gurulev (1983) suggested a metasomatic addition of Si, Al and Fe from the mafic magma to the xenolith. Mass balance calculations show that the SiO_2, TiO_2, Al_2O_3, Fe_2O_3, MnO and MgO contents of the brucite–forsterite–spinel skarns agree well with the concentration of these oxides obtained by subtraction of CaO and LOI from the original silica-poor dolomite (Table 8). Consequently, there is no need to postulate mass transfer from the mafic magma into the brucite skarns. However, Na_2O and K_2O concentrations of the brucite skarns are generally too low compared with the silica-poor dolomite precursors. Obviously, the mobile alkali elements have been lost from the xenoliths together with the calcite melt.

Reactions at the skarn–magma interface

The formation of forsterite–spinel skarns

Generally, forsterite–spinel skarns can have formed under metamorphic or magmatic conditions. A metamorphic

Table 8: Comparison of the chemical composition of Si-poor dolomite host rocks of the Ioko-Dovyren intrusion (Gurulev, 1983) with brucite/periclase–olivine–spinel skarns (Table 7); minimum and maximum content in wt %

	Si-poor dolomites, CaO- and LOI-free		Brucite/periclase–olivine–spinel skarns	
	min.	max.	min.	max.
SiO_2	2·02	19·93	4·01	17·58
TiO_2	0·11	0·47	0·04	0·23
Al_2O_3	0·92	5·47	1·59	5·33
Fe_2O_3	3·05	19·60	7·68	12·90
MnO	0·04	0·92	0·07	0·14
MgO	62·17	86·69	66·21	81·33
Na_2O	0·44	0·68	0·00	0·00
K_2O	0·07	0·60	0·00	0·01

The data for the dolomites were calculated CaO- and LOI-free to illustrate the proposed loss of calcite melt.

origin for the forsterite–spinel skarns appears to be indicated by high $\delta^{18}O$ values of skarn olivine (+16 to +19‰ SMOW). These values are just a little lower than those of dolomite host rocks (up to +24‰ SMOW, Krivoplyasov *et al.*, 1982). Several studies have observed calcite–dolomite–forsterite–spinel assemblages in the contact aureoles of silica-poor, aluminous carbonate with igneous rocks (e.g. Rice, 1977; Bowman & Essene, 1982). They were formed at low pressures of ~1 kbar and temperatures of ~600°C. The removal of calcite as a melt from this type of xenolith at relatively low temperatures (see Fig. 11) could occur only if the fluid phase was water rich. As the metamorphic breakdown of dolomite causes increasing $X(CO_2)$ of the fluid phase, calcite will probably not melt at ~600°C. A second argument against a carbonate precursor of the forsterite–spinel skarns is the relatively high Cr and Ni concentrations of these skarns (Table 7). Carbonate rocks are typically poor in Cr (~11 ppm) and Ni (20–30 ppm; Turekian & Wedepohl, 1961). Hence, it is unlikely that the composition of such skarns is simply the result of partial melting of Si-rich dolomites.

Using the MELTS software package (Ghiorso *et al.*, 1994), it was possible to demonstrate that Mg-rich olivine–spinel assemblages can crystallize from MORB-like mafic melts under specific conditions. Model spinel is generally too rich in Cr (*cr*-number ~30) and olivine is too poor in Mg (*mg*-number ~86–88) at oxygen fugacities typical for mafic magmas [around QFM (quartz–fayalite–magnetite) or NNO (nickel–nickel oxide)]. An elevated fO_2 equal to the HM buffer (haematite–magnetite) is needed to crystallize a Cr-depleted to Cr-free spinel but the crystallization path of the melt is changed to clinopyroxene → feldspar → orthopyroxene. Thus, no olivine would crystallize.

In a second model, we assumed addition of 10 wt % MgO to a fractionating MORB magma at ~1230°C and 1 kbar. This assumption is based on preliminary results of dolomite melting experiments in mafic magma (E. S. Persikov, personal communication, 2002). The experiments show that skarn periclase is partly dissolved by the magma. Model olivine with *mg*-number ~88 and model spinel with *cr*-number ~12 are predicted if the system is not buffered at a fixed oxygen fugacity. Only a model system adjusted to very high oxygen fugacity (HM) yields mineral compositions that are in agreement with the composition of olivine (*mg*-number >97) and spinel (*mg*-number ~98, *cr*-number <1·5) observed in the fine-grained forsterite–spinel skarns. Hence, if forsterite and spinel crystallized from the magma, high oxygen fugacity would be needed.

Forsterite–spinel skarns often occur as rims around the periclase skarn xenoliths, or as schlieren above Mg-skarn-bearing horizons. Hence, we investigated the effect of CO_2-rich fluids on the oxygen fugacity of the melt. We modelled the relationship between oxygen fugacity and composition of graphite-undersaturated C–O–H fluids at 1200°C and 1 kbar (see Ferry & Baumgartner, 1987; Holloway, 1987). Fugacity coefficients of H_2O, CO_2, CO, CH_4 and H_2 were calculated using modified Redlich–Kwong equations (Connolly & Cesare, 1993). The results clearly show that fluids characterized by $X(CO_2)$ >0·99 are highly oxidizing, with fO_2 equal to or higher than the HM buffer. Hence, the fO_2 of CO_2 fluids released by decarbonation reactions is high enough to cause crystallization of forsteritic olivine and Cr-free spinel from a mafic magma. We favour crystallization from melt at high fO_2, as Mg-enriched olivine and Cr-depleted spinel are also observed in dunitic cumulates adjacent to skarn xenoliths (see discussion below).

The local crystallization of monticellite and clinopyroxene within schlieren of fine-grained forsterite–spinel skarns (Fig. 2c) can be explained on the basis of the following reactions:

$$Mg_2SiO_4\ (Fo) + CaO\ (melt) \rightarrow CaMgSiO_4\ (Mtc) + MgO\ (melt) \quad (1)$$

$$CaMgSiO_4\ (Mtc) + SiO_2\ (melt) \rightarrow CaMgSi_2O_6\ (Di). \quad (2)$$

Monticellite is stable at a higher CaO activity relative to forsterite [reaction (1)], and at a lower activity of SiO_2 relative to diopside [reaction (2)]. Thus, the stability of

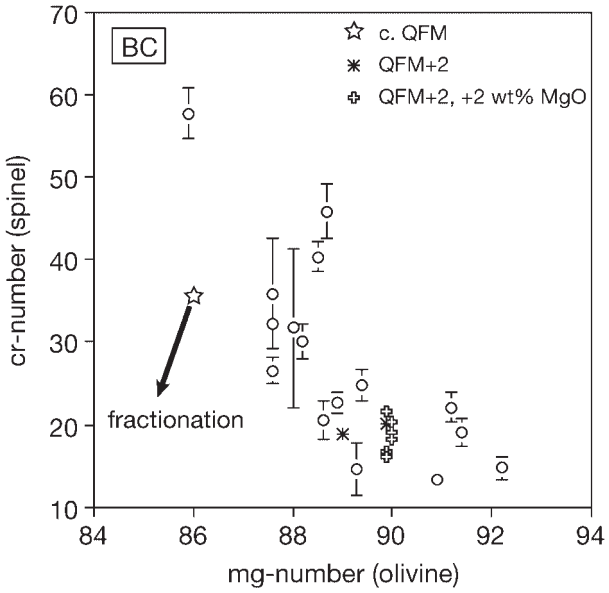

Fig. 12. Mineral compositions observed for the BC section compared with modelling results using the MELTS program (Ghiorso *et al.*, 1994). Model spinel has low *cr*-number and model olivine has high *mg*-number for crystallization from a MORB-like melt at 1 kbar and elevated $\Delta\log fO_2$ (QFM + 2). It should be noted that the *cr*-number of the first crystallizing model spinel is dependent on the Cr_2O_3 content of the model magma (0·08 wt % in our model).

both minerals depends on gradients in the CaO and SiO_2 activities at the skarn–magma interface.

The formation of Mg-enriched olivine and Cr-depleted spinel in dunites close to skarn xenoliths

Dunite samples close to skarn xenoliths (<1 m) contain olivine with elevated *mg*-number (>89·5) and spinel with lower *cr*-number (<30) compared with 'normal dunites' far from xenoliths. The chemical potential of MgO was calculated for the mineral pairs of a CaO–MgO–FeO–Al_2O_3–SiO_2 system using the PerPleX software package (Connolly, 1990) so as to understand the relationships between the several dunites. Activity corrections were made for the specific composition of olivine (two-site mixing with regular solution, $W = 4$ kJ per site), spinel (ideal mixing in inverse spinels) and clinopyroxene (*C*2/*c* Ca-pyroxene) of 'normal' dunite and dunite containing Mg-enriched olivine. However, the mineral pairs of both types of dunite are not significantly different in their chemical potentials of MgO within the uncertainty of the calculation (−645 kJ/mol for uncontaminated dunite sample 99-DV44 vs −644·2 kJ/mol for dunite 99-DV92 with Mg-rich olivine). Therefore, the Mg enrichment of olivine and the Cr depletion of spinel in dunites close to skarns cannot be simply explained by assimilation of skarn periclase by the mafic melt.

Modelling results using the program MELTS (Ghiorso *et al.*, 1994) again demonstrate the important role of the oxygen fugacity for the composition of minerals fractionating from a melt (Fig. 12). According to these calculations, the *mg*-number of model olivine would increase from ~86 at the QFM buffer to ~90 as fO_2 increases and the melt is equilibrated at QFM + 2. Using a Cr_2O_3 content of 0·08 wt % for the model melt, the *cr*-number of the spinel would decrease from ~36 to <20. Similar results are obtained if the increase in fO_2 is combined with the addition of 2 wt % MgO to the model melt.

The trends of the calculated mineral compositions are in good agreement with the trends observed in the Ioko-Dovyren dunites. For example, a correlation of increasing *mg*-number of olivine and decreasing *cr*-number of spinel is well shown in the dunites of the BC section (Fig. 12), where most of the samples are affected by contamination. Fractional crystallization of olivine and spinel would produce a different trend of decreasing *cr*-number of spinel and decreasing *mg*-number of olivine. Although it appears in Fig. 4a that the *cr*-number of spinel increases in the xenolith-rich horizons of the CC section, samples taken close to skarn xenoliths show significantly lower *cr*-number than the remaining CC samples. Again, we conclude that the increase in fO_2 reflected by the mineral data is caused by the release of metamorphic CO_2 from the skarn xenoliths (see Fig. 11, and the interpretation of the forsterite–spinel skarns). The influence of oxidizing CO_2-rich fluids must be restricted to a zone adjacent to and above the xenoliths.

Additional support for magma–xenolith interaction comes from preliminary oxygen isotope analysis (Krivoplyasov *et al.*, 1982). The $\delta^{18}O$ values of olivine from dunite adjacent to skarn xenoliths (+12 to +14‰ SMOW) are high and indicate an exchange with the assimilated dolomite rocks (up to +24‰ SMOW). CO_2 produced during the metamorphic breakdown of dolomite has a $\delta^{18}O$ value higher than that of the reacting carbonates (Valley, 1986). This ^{18}O-enriched CO_2 will, together with the calcite melt generated in the xenoliths, increase the $\delta^{18}O$ value of the coexisting mafic magma and olivine.

Mixing of calcite melt and mafic magma

The CaO enrichment of cumulus olivine

The calcite melt released from the xenoliths interacted with the surrounding mafic magma. Evidence for this process comes from the crystallization of Ca-rich olivine. There is a strong increase in the CaO content of olivine in and above the skarn horizons (Fig. 6a and b). In principle, the CaO concentration of olivine is dependent

on its forsterite content and on melt composition (Libourel, 1999; Markl *et al.*, 2001). It is particularly sensitive to the amount of calcium, aluminium, alkali and ferrous iron in the coexisting melt, but not to the temperature of formation. There is a restricted range in the *mg*-number of olivine (86–92), which does not correlate with the CaO content. In addition, there is no evidence for variable Al_2O_3, Na_2O and K_2O contents in the parental magma during crystallization of the dunite cumulates (Table 6). Hence, the increase in CaO of olivine is related to an increase of the CaO activity of the melt and/or a decrease of a_{SiO_2}. Qualitative estimates using MELTS (Ghiorso *et al.*, 1994) show that addition of 4 wt % CaO to the parental magma will increase CaO in olivine to 0·59 wt % at 1230°C and 1 kbar. Addition of 4 wt % CaO to the magma at a lower pressure of 0·3 kbar causes an even higher content of 0·64 wt % CaO of olivine with *mg*-number 82–83. Addition of >4 wt % CaO would change the crystallization path and induce abundant precipitation of clinopyroxene.

The crystallization of CaO-rich olivine also depends on the volume of fractionating mafic magma that could be enriched in CaO by mixing with the calcite melt. If there was a large stagnating magma volume, as might be the case on top of the skarn-rich horizon II in the CC section, a thick zone of CaO-rich cumulus olivine could form (Fig. 6a). If, in contrast, injections of fresh, NiO-rich basalt led to a rapid dilution of the contaminated magma (as probably occurred within and above horizon I in CC), the CaO enrichment of olivine is much less pronounced. Although olivine in the BC section is generally rich in CaO (Fig. 6b), the highest concentrations are observed on top of the xenolith-bearing zone between 300 and 375 m. As in the CC section, the zone with CaO-rich olivine is characterized by low NiO concentrations, indicating a stagnant volume of fractionating mafic magma (Fig. 6b).

The formation of Cats-rich intercumulus clinopyroxene

A further important consequence of the mixing of mafic and calcite melt is the crystallization of intercumulus clinopyroxene enriched in the Ca-Tschermak's component (Figs 8 and 9). In the following, we use the pressure- and temperature-sensitive equilibrium constant K of the reaction

$$SiO_2\ (melt) + CaAl_2SiO_6\ (Cpx) \rightarrow CaAl_2Si_2O_8\ (Pl) \quad (3)$$

to estimate the influence of calcite assimilation on the silica activity of the magma. The K value used in our calculations is from experimental calibrations of the reaction by McCarthy & Patiño Douce (1998). Mole fractions and activities of An and Cats were calculated according to McCarthy & Patiño Douce (1998). A pressure of 1 kbar and a temperature of 1180°C were assumed. A fixed plagioclase composition of An_{100} was used for modelling, as most of the contaminated dunite samples do not contain plagioclase. As the actual activity of anorthite is lower than that used in the calculation, the calculated silica activities are maximum values. Nevertheless, the contaminated samples are characterized by lower SiO_2 activities compared with the uncontaminated dunites from the lower part of CC. This result is in agreement with conclusions on a 'desilication' of mafic magma as a result of the addition of CaO from broken-down carbonate (e.g. Daly, 1910; Joesten, 1977).

Overall, the observed changes in mineral composition of the dunites are consistent with contamination of the mafic magma with CaO. The source of the CaO is probably a calcite melt formed during the interaction of dolomite xenoliths with mafic silicate magma. This conclusion is based on field relationships and coincidence of occurrence, although any evidence for calcite melting in the strict sense cannot be provided.

SUMMARY

On the basis of complex field and petrological investigations, we propose the following model for the formation of the Mg-rich skarns from dolomite xenoliths and the contamination of the basaltic magma (Fig. 13).

Rapid heating of the xenoliths after incorporation into the mafic magma caused decomposition of dolomite to calcite + periclase + CO_2, and, progressively, melting of calcite. Such partial melting has been predicted by experimental results (Wyllie, 1965) to occur in contact metamorphism. But so far, it has never been detected in nature. Calcite melt was squeezed out of the xenolith, as it has a low viscosity and a low density. Xenoliths collapsed by $\sim$70% in volume.

Mixing of mafic magma and calcite melt resulted in the crystallization of cumulus olivine with high CaO content and of intercumulus clinopyroxene enriched in the $CaAl_2SiO_6$ component. Metamorphic CO_2 fluids released from the xenoliths led to increasing oxygen fugacities in the neighbourhood of the skarns. Dunitic cumulates containing very Mg-rich olivine and Cr-poor spinel, and fine-grained forsterite–spinel skarns formed at high fO_2 in the neighbourhood of decomposing xenoliths. Saturation of the magma with a Ca-bearing phase (Cpx) caused the crystallization of monticellite and clinopyroxene in the forsterite–spinel skarn schlieren. Stabilization of Ca minerals reflects the increasing activity of CaO during the final stage of skarn formation.

Our results demonstrate that carbonate contamination can dramatically affect the redox state of the crystallizing magma. As a consequence, Mg-rich olivine will crystallize, which could be erroneously interpreted to indicate

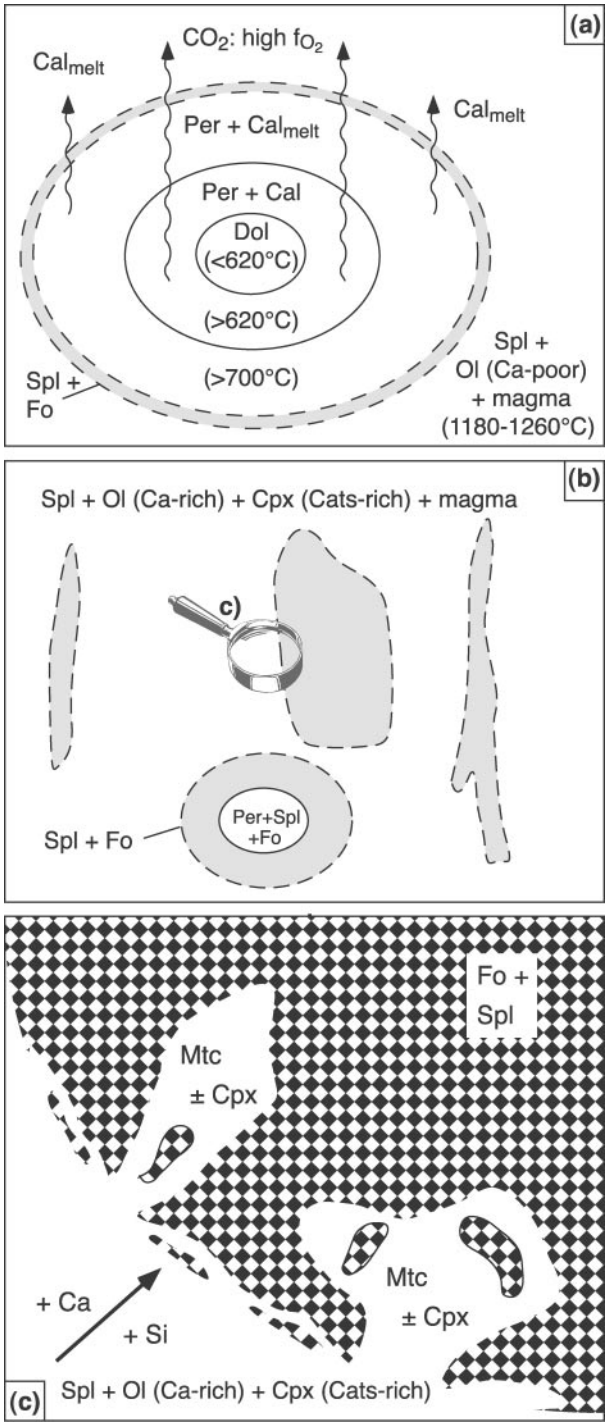

Fig. 13. A model for the metamorphic evolution of Mg-rich skarns from dolomitic precursors and the contamination of mafic magma by mixing with calcite melt [modified after Wenzel *et al.* (2001)] (see text for discussion and the Appendix for mineral abbreviations).

komatiitic affinities of the parental magma. Detailed geological and mineralogical investigations are necessary to exclude carbonate contamination and to reconstruct potential mantle source characteristics of the mafic magma.

ACKNOWLEDGEMENTS

Reviews by B. W. D. Yardley, G. Markl, M. Amelio Logon and J. Wolff significantly improved the paper. Technical support by B. Schulz-Dobrick and N. Groschopf with XRF and microprobe analyses is acknowledged. We thank C. Hauzenberger and R. Fernando for helpful discussions. Graphical styling of the figures by G. Feyerherd is very appreciated. Financial support was provided by Deutsche Forschungsgemeinschaft (DFG grant Ba 1876/1 to L.P.B.) and by the Russian Science Foundation (RFBR grant 99-05-04013 to E.G.K. and E.V.K.).

REFERENCES

Alexandrov, S. M. (1990). *The Geochemistry of Skarns and Ores in Dolomites* (in Russian). Moscow: Nauka.

Amelin, Yu. V., Neymark, L. A., Ritsk, E. Yu. & Nemchin, A. A. (1996). Enriched Nd–Sr–Pb isotopic signatures in the Dovyren layered intrusion (eastern Siberia, Russia): evidence for source contamination by ancient upper-crustal material. *Chemical Geology* **129**, 39–69.

Baker, C. K. & Black, P. M. (1980). Assimilation and metamorphism at a basalt–limestone contact, Tokatoka, New Zealand. *Mineralogical Magazine* **43**, 797–807.

Bowman, J. R. & Essene, E. J. (1982). *P–T–X*(CO_2) conditions of contact metamorphism in the Black Butte aureole, Elkhorn, Montana. *American Journal of Science* **282**, 311–340.

Bucher, K. & Frey, M. (1994). *Petrogenesis of Metamorphic Rocks*, 6th edn. Berlin: Springer, pp. 309–310.

Cameron, W. E. & Nisbet, E. G. (1982). Phanerozoic analogues of komatiitic basalts. In: Arndt, N. T. & Nisbet, E. G. (eds) *Komatiites*. London: George Allen & Unwin, pp. 29–50.

Carslaw, H. S. & Jaeger, J. C. (1959). *Conduction of Heat in Solids*, 2nd edn. Oxford: Clarendon Press, pp. 233–234.

Connolly, J. A. D. (1990). Multivariate phase diagrams: an algorithm based on generalized thermodynamics. *American Journal of Science* **290**, 666–718.

Connolly, J. A. D. & Cesare, B. (1993). C–O–H–S fluid composition and oxygen fugacity in graphitic metapelites. *Journal of Metamorphic Geology* **11**, 379–388.

Daly, R. A. (1910). Origin of the alkaline rocks. *Geological Society of America Bulletin* **21**, 87–118.

Dick, H. J. B. & Bullen, T. (1984). Chromian spinel as a petrogenetic indicator in abyssal and alpine-type peridotites and spatially associated lavas. *Contributions to Mineralogy and Petrology* **86**, 54–76.

Droop, G. T. R. (1987). A general equation for estimating Fe^{3+} concentrations in ferromagnesian silicates and oxides from microprobe analyses, using stoichiometric criteria. *Mineralogical Magazine* **51**, 431–435.

Efimov, A. A., Kolyasnikov, A. A., Mayegov, V. I., Yablonskaya, L. V. & Potapova, T. A. (1986). The occurrence of Ti-fassaite + perovskite associations in Mg-skarns of the Ioko-Dovyren intrusion (North Baikal region) (in Russian). *Institute of Geology and Geochemistry Sverdlovsk, Yearbook* **1985**, 92–94.

Ferry, J. M. & Baumgartner, L. (1987). Thermodynamic models of molecular fluids at the elevated pressures and temperatures of crustal metamorphism. In: Carmichael, I. S. E. & Eugster, H. P. (eds) *Thermodynamic Modelling of Geological Materials: Minerals, Fluids and Melts. Mineralogical Society of America, Reviews in Mineralogy* **17**, 323–365.

Francis, D. (1994). Chemical interaction between picritic magma and upper crust along the margins of the Muskox intrusion, Northwest Territories. *Geological Survey of Canada Paper* **92-12**.

Genge, M. J., Price, G. D. & Jones, A. P. (1995). Molecular dynamics simulations of $CaCO_3$ melts to mantle pressures and temperatures: implications for carbonatite magmas. *Earth and Planetary Science Letters* **131**, 225–238.

Ghiorso, M. S., Hirschmann, M. M. & Sack, R. O. (1994). New software models—thermodynamics of magmatic systems. *EOS Transactions, American Geophysical Union* **75**, 574–576.

Gray, C. M., Cliff, R. A. & Goode, A. D. T. (1981). Neodymium–strontium isotopic evidence for extreme contamination in a layered basic intrusion. *Earth and Planetary Science Letters* **56**, 189–198.

Green, D. H. & Ringwood, A. E. (1967). The genesis of basaltic magmas. *Contributions to Mineralogy and Petrology* **15**, 103–190.

Gurulev, S. A. (1983). *Conditions of Formation of Mafic Layered Intrusions*. Moscow: Nauka.

Hart, S. R. & Davis, K. E. (1978). Nickel partitioning between olivine and silicate melt. *Earth and Planetary Science Letters* **40**, 203–219.

Holland, T. J. B. & Powell, R. (1998). An internally consistent thermodynamic data set for phases of petrological interest. *Journal of Metamorphic Geology* **16**, 309–343.

Holloway, J. R. (1987). Igneous fluids. In: Carmichael, I. S. E. & Eugster, H. P. (eds) *Thermodynamic Modelling of Geological Materials: Minerals, Fluids and Melts. Mineralogical Society of America, Reviews in Mineralogy* **17**, 211–233.

Huppert, H. E. & Sparks, R. S. J. (1985). Cooling and contamination of mafic and ultramafic magmas during ascent through continental crust. *Earth and Planetary Science Letters* **74**, 371–386.

Irvine, T. N. (1980). Magmatic infiltration metasomatism, double-diffusive fractional crystallization, and adcumulus growth in the Muskox intrusion and other layered intrusions. In: Hargraves, R. B. (ed.) *Physics of Magmatic Processes*. Princeton, NJ: Princeton University Press, pp. 325–383.

Irvine, T. N. (1982). Terminology for layered intrusions. *Journal of Petrology* **23**, 127–162.

Joesten, R. (1977). Mineralogical and chemical evolution of contaminated igneous rocks at a gabbro–limestone contact, Christmas Mountains, Big Bend region, Texas. *Geological Society of America Bulletin* **88**, 1515–1529.

Joesten, R., Hill, J. & Van-Horn, S. R. (1994). Limestone assimilation and clinopyroxenite production along the contacts of a 9 metre alkali olivine basalt dike, Killala Bay, Ireland. *Geological Society of America, Abstracts with Programs* **26**, 476.

Kimball, K. L. (1990). Effects of hydrothermal alteration on the compositions of chromian spinels. *Contributions to Mineralogy and Petrology* **105**, 337–346.

Kislov, E. V. (1998). *Ioko-Dovyren Layered Massif* (in Russian). Ulan-Ude: RAS SD Buryat Scientific Publishing House.

Konnikov, E. G., Kislov, E. V. & Kacharovskaya, L. N. (1988). New data on the petrology and the ore content of the Yoko-Dovyren nickel-bearing pluton. *Soviet Geology and Geophysics* **29**, 33–41.

Konnikov, E. G., Kislov, E. V. & Orsoev, D. A. (1994). Ioko-Dovyren layered pluton and associated ore mineralization (Northern part Pri-Baikal region). *Geology of Ore Deposits* **36**, 490–498.

Krivoplyasov, G. S., Yaroshevsky, A. A., Ustinov, V. I. & Strizhov, V. P. (1982). Redistribution of oxygen isotopes during the interaction of a magmatic system with enclosed rocks. *9th All-Union Symposium on Stable Isotope Geochemistry* **1**, 134–136.

Libourel, G. (1999). Systematics of calcium partitioning between olivine and silicate melt: implications for melt structure and calcium content of magmatic olivines. *Contributions to Mineralogy and Petrology* **136**, 63–80.

Lloyd, F. E. & Bailey, D. K. (1975). Light element metasomatism of the continental mantle: the evidence and the consequences. *Physics and Chemistry of the Earth* **9**, 389–416.

Maier, W. D., Arndt, N. T. & Curl, E. A. (2000). Progressive crustal contamination of the Bushveld Complex: evidence from Nd isotopic analyses of the cumulate rocks. *Contributions to Mineralogy and Petrology* **140**, 316–327.

Markl, G., Marks, M. & Wirth, R. (2001). The influence of T, a_{SiO_2}, and fO_2 on exsolution textures in Fe–Mg olivine: an example from augite syenites of the Illimausaq intrusion, South Greenland. *American Mineralogist* **86**, 36–46.

McCarthy, T. C. & Patiño Douce, A. E. (1998). Empirical calibration of the silica Ca-Tschermak's–anorthite (SCAn) geobarometer. *Journal of Metamorphic Geology* **16**, 675–686.

Miyashiro, A. (1974). Volcanic rock series in island arcs and active continental margins. *American Journal of Science* **274**, 321–355.

Morimoto, N. (1988). Nomenclature of pyroxenes. *Mineralogical Magazine* **52**, 535–550.

Mysen, B. O. & Boettcher, A. L. (1975). Melting of a hydrous mantle: II. Geochemistry of crystals and liquids formed by anatexis of mantle peridotite at high pressures and high temperatures as a function of controlled activities of water, hydrogen and carbon dioxide. *Journal of Petrology* **16**, 549–593.

Naldrett, A. J. (1989). Sulfide melts: crystallization temperatures, solubility in silicate melts, and Fe, Ni, and Cu partitioning between basaltic magmas and olivine. In: Whitney, J. A. & Naldrett, A. J. (eds) *Ore Deposition Associated with Magmas. Review of Economic Geology* **4**, 5–20.

Neimark, L. A., Ritsk, E. Yu., Gorokhovsky, B. M., Ovchinnikova, G. V., Kiseleva, E. I. & Konkin, V. D. (1991). Lead isotopic composition and genesis of Pb–Zn ores in the Olokit zone, North Baikal region (in Russian). *Geology of Ore Deposits* **33**, 34–49.

Owens, B. E. (2000). High-temperature contact metamorphism of calc-silicate xenoliths in the Kiglapait Intrusion, Labrador. *American Mineralogist* **85**, 1595–1605.

Papunen, H., Distler, V. & Sokolov, A. (1992). PGE in the upper Proterozoic Dovirensky layered complex, North Baikal area, Siberia. *Australian Journal of Earth Sciences* **39**, 327–334.

Patchett, P. J. (1980). Thermal effects of basalt on continental crust and crustal contamination of magmas. *Nature* **283**, 559–561.

Pertzev, N. N. & Shabynin, L. I. (1979). Skarn, carbonate and brucite xenoliths of the Ioko-Dovyren massif. In: Korzhinskiy, D. S., Gurulev, S. A. & Zotov, I. A. (eds) *Contact Processes and Mineralization at Gabbro–Peridotite Intrusions* (in Russian). Moscow: Nauka, pp. 85–96.

Puchtel, I. S., Haase, K. M., Hofmann, A. W., Chauvel, C., Kulikov, V. S., Garbe-Schönberg, C.-D. & Nemchin, A. A. (1997). Petrology and geochemistry of crustally contaminated komatiitic basalts from the Vetreny Belt, southeastern Baltic Shield: evidence for an early Proterozoic mantle plume beneath rifted Archean continental lithosphere. *Geochimica et Cosmochimica Acta* **61**, 1205–1222.

Reiners, P. W., Nelson, B. K. & Nelson, S. W. (1996). Evidence for multiple mechanisms of crustal contamination of magma from compositionally zoned plutons and associated ultramafic intrusions of the Alaska Range. *Journal of Petrology* **37**, 261–292.

Rice, J. M. (1977). Contact metamorphism of impure dolomitic limestone in the Boulder aureole, Montana. *Contributions to Mineralogy and Petrology* **59**, 237–259.

Roeder, P. L. & Emslie, R. F. (1970). Olivine–liquid equilibrium. *Contributions to Mineralogy and Petrology* **29**, 275–289.

Sack, R. O. & Ghiorso, M. S. (1991). Chromian spinels as petrogenetic indicators: thermodynamics and petrological applications. *American Mineralogist* **76**, 827–847.

Shand, S. J. (1930). Limestone and the origin of feldspathoidal rocks: an aftermath of the Geological Congress. *Geological Magazine or Monthly Journal of Geology* **67**, 415–427.

Stewart, B. W. & DePaolo, D. J. (1992). Diffusive isotopic contamination of mafic magma by coexisting silicic liquid in the Muskox intrusion. *Science* **255**, 708–711.

Sun, S.-S., Nesbitt, R. W. & Sharaskin, A. Ya. (1979). Geochemical characteristics of mid-ocean ridge basalts. *Earth and Planetary Science Letters* **44**, 119–138.

Tegner, C., Robins, B., Reginiussen, H. & Grundvig, S. (1999). Assimilation of crustal xenoliths in a basaltic magma chamber: Sr and Nd isotopic constraints from the Hasvik layered intrusion, Norway. *Journal of Petrology* **40**, 363–380.

Thirlwall, M. F. & Jones, N. W. (1983). Isotope geochemistry and contamination mechanics of Tertiary lavas from Skye, northwest Scotland. In: Hawkesworth, C. J. & Norry, M. J. (eds) *Continental Basalts and Mantle Xenoliths*. Shiva: Nantwich, pp. 186–208.

Thompson, R. N., Morrison, M. A., Hendry, G. L. & Parry, S. J. (1984). An assessment of the relative roles of a crust and mantle in magma genesis: an elemental approach. *Philosophical Transactions of the Royal Society of London, Series A* **310**, 549–590.

Tilley, C. E. (1952). Some trends of basaltic magma in limestone syntexis. *American Journal of Science* **250A**, 529–545.

Turekian, K. K. & Wedepohl, K. H. (1961). Distribution of the elements in some major units of the Earth's crust. *Geological Society of America Bulletin* **72**, 175–192.

Turner, J. S. & Campbell, I. H. (1986). Convection and mixing in magma chambers. *Earth-Science Reviews* **23**, 255–352.

Valley, J. W. (1986). Stable isotope geochemistry of metamorphic rocks. In: Valley, J. W., Taylor, H. P., Jr & O'Neil, J. R. (eds) *Stable Isotopes in High Temperature Geological Processes. Mineralogical Society of America, Reviews in Mineralogy* **16**, 445–489.

Wenzel, Th., Mertz, D. F., Oberhänsli, R., Becker, T. & Renne, P. R. (1997). Age, geodynamic setting, and mantle enrichment processes of a K-rich intrusion from the Meissen massif (northern Bohemian massif) and implications for related occurrences from the mid-European Hercynian. *Geologische Rundschau* **86**, 556–570.

Wenzel, T., Baumgartner, L. P., Brügmann, G. E., Konnikov, E. G., Kislov, E. V. & Orsoev, D. A. (2001). Partial melting and assimilation of dolomitic xenoliths by mafic magma. *Terra Nova* **13**, 197–202.

Wilson, M. (1989). *Igneous Petrogenesis*. London: Unwin Hyman, pp. 1–466.

Wyllie, P. J. (1965). Melting relationships in the system CaO–MgO–CO_2–H_2O, with petrological applications. *Journal of Petrology* **6**, 101–123.

Yaroshewskiy, A. A., Mironov, Y. V., Ionov, D. A., Abramov, A. V., Krivoplyasov, G. S., Koptev-Dvornikov, E. V. & Barmina, G. S. (1983). Internal structure of the Yoko-Dovyren dunite–troctolite–gabbro–norite massif. In: *Magmatism and Metamorphism of the BAM Area* (in Russian). Novosibirsk: Nauka, pp. 161–168.

APPENDIX

Symbols for minerals used in the text, mainly after Bucher & Frey (1994)

Ab	albite	Merw	merwinite
Am	amphibole	Mtc	monticellite
An	anorthite	Ol	olivine
Brc	brucite	Or	orthoclase
Cal	calcite	Per	periclase
Cats	Ca-Tschermak	Pl	plagioclase
Cpx	clinopyroxene	Qtz	quartz
Di	diopside	Spl	spinel
Dol	dolomite	Tr	tremolite
Fo	forsterite		